



## Master's Thesis

# Effekt des Antibiotikums Kirromycin auf den Elongations Faktor Tu untersucht mit Molekulardynamik-Simulationen

## Effect of the antibiotic kirromycin on elongation factor Tu studied through molecular-dynamics simulations

prepared by

**Malte Varias**

from Braunschweig

at the Max Planck Institute for Biophysical Chemistry

**Thesis period:** 11th May 2017 until 11th November 2017

**Supervisor:** Prof. Dr. Helmut Grubmüller

**First Rreferee:** Prof. Dr. Helmut Grubmüller

**Second referee:** Prof. Dr. Marcus Müller



# Contents

<b>1</b>	<b>Introduction</b>	<b>1</b>
1.1	Biological Background . . . . .	1
1.1.1	Ribonucleic acid . . . . .	1
1.1.2	Proteins . . . . .	3
1.1.3	Ribosome . . . . .	4
1.1.4	Elongation Factor Thermally unstable . . . . .	6
1.1.5	Kirromycin . . . . .	9
<b>2</b>	<b>Methods</b>	<b>11</b>
2.1	Molecular Dynamics Simulations . . . . .	11
2.1.1	Equations of motion . . . . .	11
2.1.2	Integration of Newton equations for the nuclei . . . . .	15
2.2	Secondary Structure Analysis . . . . .	16
2.3	Root Mean Square Deviation . . . . .	17
2.4	Principal Component Analysis . . . . .	17
2.5	Sequence Alignment . . . . .	19
2.6	Umbrella sampling . . . . .	19
2.7	System Set-up . . . . .	22
2.7.1	Ribosomal simulations . . . . .	22
2.7.2	Free simulations . . . . .	22
<b>3</b>	<b>Results</b>	<b>25</b>
3.1	Influence of Kirromycin on EF-Tu dynamics . . . . .	25
3.1.1	Quaternary dynamics change of EF-Tu . . . . .	25
3.1.2	Switch 1 secondary structure behaviour . . . . .	27
3.1.3	Validity of switch 1 structure . . . . .	31
3.2	Kirromycin-free EF-Tu dynamics . . . . .	33
3.2.1	Umbrella sampling . . . . .	35



# 1 Introduction

Bacteriostatic antibiotics do not actively kill bacteria, they prevent their growth. A common target for this type of antibiotic is the translation process. During translation, genetic information is decoded and used as a blueprint by the ribosome to synthesize proteins. Without the capability of producing new proteins, the natural decay of existing ones kills the bacterium.

Kirromycin is a bacteriostatic antibiotic. It was first extracted from *Streptomyces collinus* in 1972[48]. Two years later it was shown that it binds to Elongation Factor Tu (EF-Tu) and causes translation to shutdown by preventing EF-Tu from dissociating from the ribosome[49]. EF-Tu's main task during translation is to deliver aminoacyl-tRNA, carriers of the building blocks from which proteins are formed, to the ribosome. After the discovery of kirromycin's binding site[1], it was quickly proposed to hinder EF-Tu's dynamics, preventing it from changing its conformation from GTP to GDP state.

Although the overall motion prevented by kirromycin is known, the molecular mechanism of this hinderance is less clear. MD simulations with their unique ability to study the dynamics of proteins on atomistic scales, without being limited by experimental constraints like measuring dead times during sample preparation, will be used to test if kirromycin does hinder the dynamics, and if so in what way.

## 1.1 Biological Background

### 1.1.1 Ribonucleic acid

Ribonucleic acid (RNA) is a polymer of nucleotides, and is one of the major macromolecules comprising all cells, along with DNA, proteins, lipids and carbohydrates. RNA can form versatile structures and perform various functions in a cell. Structurally, nucleotides are build of a ribose and phosphate backbone to which one of four bases is bound[18] (see figure 1.1a). These bases are guanine, adenine, cytosine

## 1 Introduction

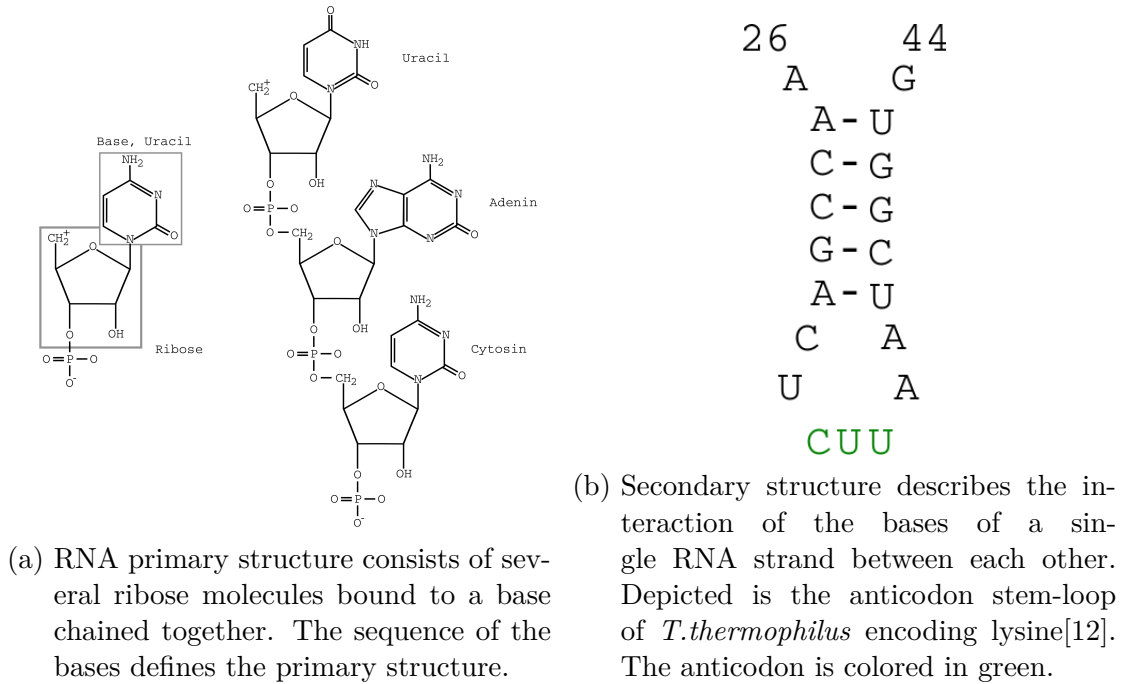


Figure 1.1: Primary and secondary structure of RNA are depicted.

and uracil. Uracil is the unmethylated form of thymine, the fourth base found in DNA. A major task of RNA is the encoding of genetic information to be translated into a protein (see section 1.1.2) by the ribosome (see section 1.1.3). During translation alone, three types of RNA are used: the messenger RNA (mRNA) that contains the genetic information, the transfer RNA (tRNA) that binds to an amino acid, the building blocks of proteins, and the ribosomal RNA (rRNA) which forms the ribosome, the molecular machine in which the amino acids are linked together. While all these forms of RNA are built from the same four ribose-bound nucleic acids, they differ in their structure. RNA structure is generally described by primary and secondary structure (see figure 1.1). This structure is essential for the RNAs function. For example, an anticodon is a three nucleotides long sequence that matches the codon of the mRNA, which encodes the information which amino acid should be incorporated next, during protein translation. The anticodon stem-loop of tRNA is depicted in figure 1.1b, its secondary hairpin structure stabilizes the positions of the anticodon bases. A stable three dimensional structure is important for the tRNA and the anticodon because to translate the genetic code it has to precisely positioned in order to base pair with an mRNA nucleotide triplet (codon).

### 1.1.2 Proteins

Proteins are long chains of amino acids performing a wide variety of functions in cells. Amino-acids are organic molecules which all share a common backbone (see figure 1.2), which can attach to other amino acids by peptide bond formation. Like the base of RNA, differences in amino acids occur in their residue, which defines chemical and physical properties. Twenty different types of amino acids are known to be coded by mRNA codons and are generally classified by their properties into nonpolar and polar, and the latter into charged and uncharged polar amino acids. In all organisms, proteins perform essential functions like the oxygen transport of hemoglobin in mammals. To perform these functions, the structure of a protein is important.

This protein structure is described by four levels, the first two of which are equivalent to the primary and secondary structure of RNA.

The primary structure is the amino acid sequence they consist of. It is stabilized by the covalent peptide bonds.

In the secondary structure information about the local arrangement of the amino acids is contained. The most common motives are helices and  $\beta$ -sheets (see figure 2.2). These two structures are formed by hydrogen bonds of the backbones of the amino acids.

Tertiary structure describes the three dimensional folding of the local arrangement. There are various interaction types that change the free energy landscape this folding takes place in.

Molecules not part of the amino acid sequence, for example ions, can also physically bind to the protein and have an effect on the structure.

Proteins structure can often be separated into different domains of a single strand of amino acids, larger proteins can also consist of multiple subunits that are non-covalently bound (e.g. hemoglobin, which consists of 4 such subunits). The orientation of these domains and subunits against each other is called quaternary structure (see figure 1.5 for an example).

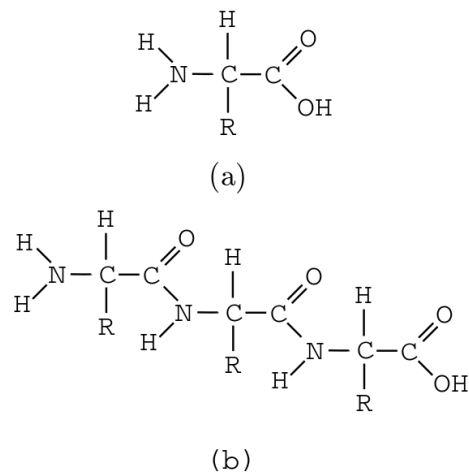


Figure 1.2: Chemical structure of a protein backbone. (a) shows a single amino acid, (b) three amino acids connected through peptide bonds.

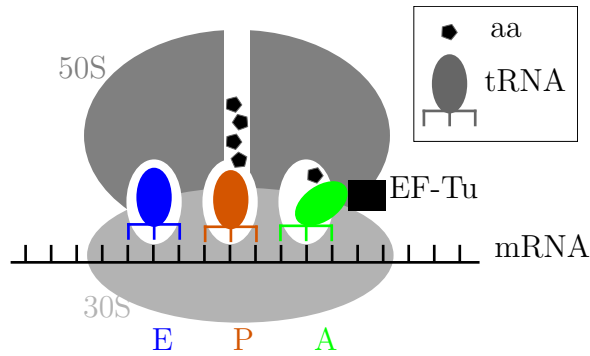


Figure 1.3: Shown is a schematic 70S ribosome. It consists of two subunits, the mRNA containing 30S and the 50S subunit, which contains the PTC. The depicted state is after codon recognition during elongation but before GTPase activation.

### 1.1.3 Ribosome

The ribosome is a molecular machine that produces proteins by catalysing peptide bond formation of amino acids. Amino acids are selected by matching of the anticodon, found on the tRNA carrying the amino acid, to the codon of the mRNA. The bacterial ribosome consists of three rRNAs, but also contains 54 proteins[47]. Most ribosomal proteins are located on the surface while the rRNA forms a core which contains the tRNA binding site and the catalytic site. The ribosome is composed of two subunits (a sketch is in figure 1.3), the large and the small subunit, or 50S and 30S subunit for bacterial 70S ribosomes. <sup>1</sup>. The mRNA lies in the small subunit, which is associated with ensuring correct codon-anticodon pairing while the large subunit contains the peptidyltransferase center (PTC) and is responsible for extending the amino acid chain. In between the two subunits are the Aminoacyl, Peptidyl and Exit sites in which the tRNAs are bound.

Bacterial translation is divided into three separate phases,

1. initiation: the ribosome assembles around the mRNA, the initiator tRNA is incorporated in the *P*-site over the start codon,
2. elongation: the nascent chain is extended by repeatedly adding amino acids to it by a cycle of decoding the mRNA, peptide-bond formation between the nascent chain and the amino acid of the tRNA in the A-site and translocation, and

---

<sup>1</sup>S is here the unit Svedberg, a unit for the sedimentation coefficient.

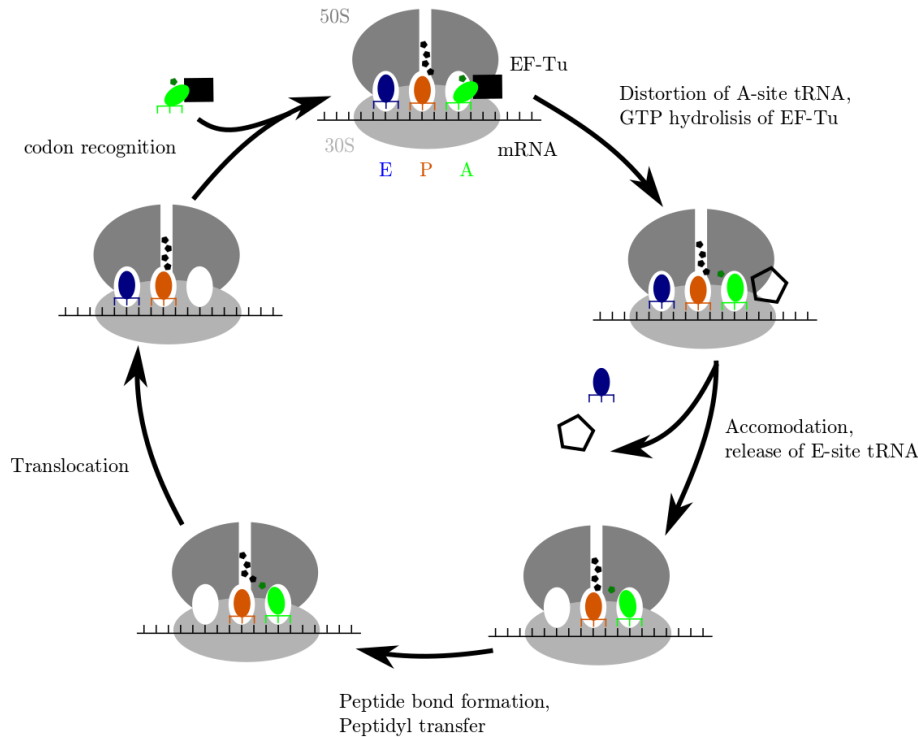


Figure 1.4: The elongation cycle is sketched. For a description see section 1.1.3.

3. termination: in the A-site the mRNA codon is a stop codon, the nascent chain is then cleaved from the P-site tRNA and the synthesized protein leaves the ribosome, which disassembles.

## Elongation

Elongation is a three step cycle that adds a single amino acid to the nascent chain per repetition (figure 1.4). It occurs after initiation and continues until the mRNA codon in the A-site is a stop codon.

During the first step, decoding, an aminoacyl-tRNA in complex with EF-Tu is inserted into the A-site. If the anticodon of the tRNA does not match the mRNA codon, the tRNA · EF-Tu complex leaves the ribosome again. This process has error rates of around 1 in  $10^4$ , these low error rates are achieved through free energy differences between correct and wrong codon-anticodon pairings, kinetic proofreading[10] and an accelerated GTP hydrolysis rate of EF-Tu for correct pairings[16]. After initial binding of the EF-Tu·tRNA complex the tRNA is distorted so that it can interact with EF-Tu and the decoding center of the 30S subunit at the same time[37]. Correct codon recognition is transmitted to EF-Tu, which could causes conformational

## 1 Introduction

changes which trigger GTP hydrolysis.[36]. EF-Tu is released from the ribosome and the tRNA fully accommodates into the A-site.

The ribosome catalyses the peptide bond formation between the nascent chain bound to the P-site tRNA and the amino acid on the A-site tRNA by a factor of  $10^7$ [39], compared to non catalysed peptide bond formation. Peptide bond formation also transfers the nascent chain to the A-site tRNA. The parts of P and A-site tRNA embedded in the 50S subunit spontaneously assume hybrid states between P/E and A/P site. Elongation Factor G facilitates translocation, leading to a change also with respect to the 30S subunit[29]. This leaves the ribosome in a post-initiation state, from which the elongation cycle is repeated until a stop codon is reached on the mRNA.

### 1.1.4 Elongation Factor Thermally unstable

Elongation Factor Thermally unstable (EF-Tu) is facilitating aa-tRNA binding to the A-site of the ribosome during the decoding step of elongation. It is one of the most plentiful proteins in bacteria (making up 5-11% of protein numbers in *E. Coli*) and highly conserved across different species[46]. EF-Tu consists of three domains and around 390 amino acids, depending on the species (393 for *E. Coli*). The amino acid numbering for *E. Coli* EF-Tu will be used in this work. The GTP binding domain 1 is the largest with around 200 amino acids, the other two are both close to 100 amino acids long. Domain 1's structure is common for GTP binding domains with six  $\beta$ -sheets surrounded by six  $\alpha$ -helices. The domain also contains the switch regions consisting of switch 1 and switch 2, both of which are thought to be important for tRNA and ribosome interactions. Switch 1 consists, in GTP conformation, of two  $\alpha$ -helices, the second of which is close to the 3' end of the tRNA. After GTP hydrolysis the domain undergoes large conformational changes, including the secondary structure of the switch regions[2][37]. In the GTP conformation, the tRNA is bound to EF-Tu through interactions with all three domains. The amino acid of the aa-tRNA sits in a pocket between domain 1 and 2 formed by His<sup>66</sup> and Glu<sup>229</sup>[33]. Different other interactions are present, depending on the amino acid. Residues 229-236 and 272-277 form a pocket in which the 3' end of the tRNA binds. The 5' end binds in the junction of all three domains, interacting closely with residues 55-59, parts of the switch 1 loop. It further interacts with the residues 85-88, 90+91, 300-303 and 346-348[33].

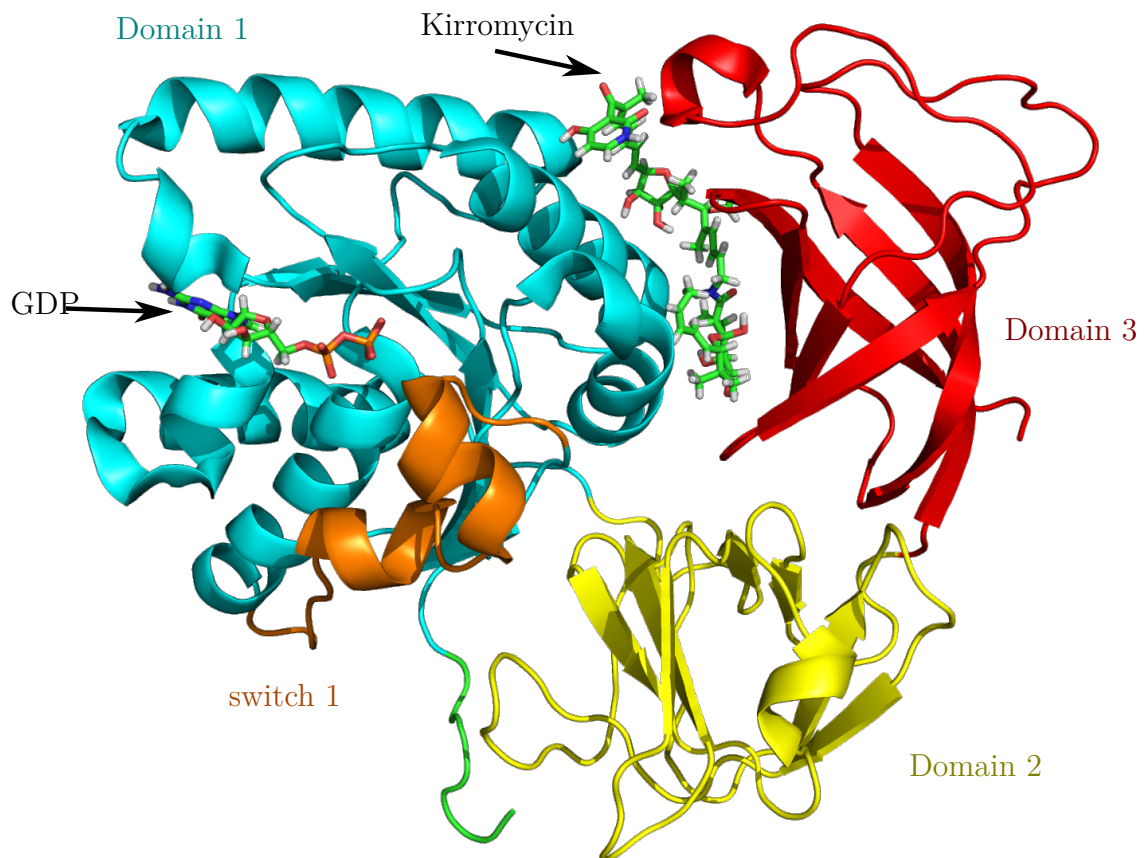


Figure 1.5: Structure of EF-Tu in complex with GDP and kirromycin[13] depicted as ribbons. The structure is coloured according to the domains with the switch 1 loop highlighted in orange.

## 1 Introduction

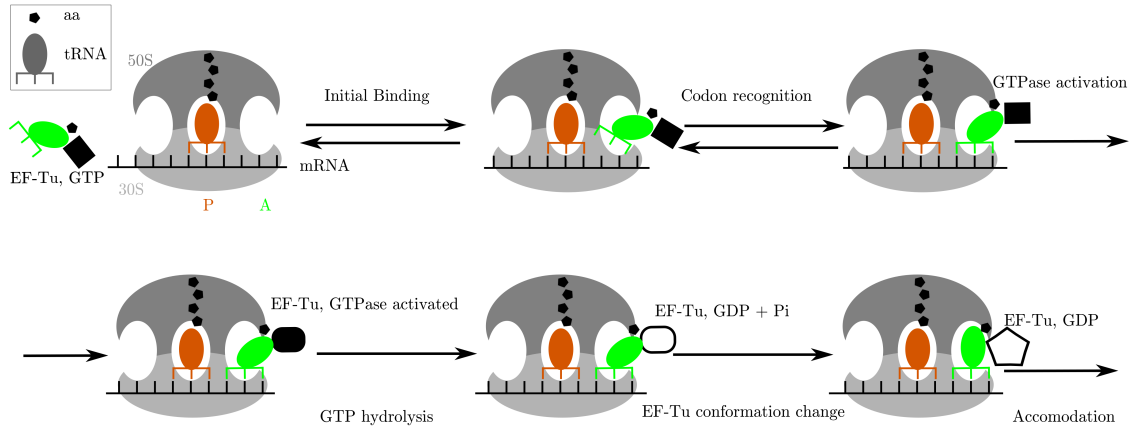


Figure 1.6: The mechanism of EF-Tu dependant aa-tRNA binding to the ribosome is sketched.

### Function during decoding

EF-Tu helps with incorporation of aa-tRNA into the A-site and is also involved with ensuring high translational accuracy (compare [35]). aa-tRNA binding of EF-Tu is specific to cognate amino acid and tRNA pairs. Misacylated tRNAs where the amino acid is smaller than the cognate one bind poorly to EF-Tu, and are likely released from EF-Tu before they are inserted into the ribosome[26]. The first step of decoding is the initial binding of the ternary complex of EF-Tu · tRNA · GTP to the ribosome. This is facilitated by the stalk on the 50S subunit formed by proteins L7/12 interacting with EF-Tu[24]. tRNA out of complex binds at a far slower rate[10]. Afterwards codon recognition occurs, through a number of intermediate states, forming a contact between codon and anticodon and rearranging the 16S rRNA[34]. The rate of codon recognition is similar for cognate and near-cognate codon-anticodon pairs, however mismatched pairs have a higher rate of disassociation. For GTPase activation, the aa-tRNA is moved further into the A-site into a strained conformation[10] until 30S subunit closes, bringing its shoulder into closer contact with EF-Tu. The aa-tRNA is overall in a more open conformation, stabilized by interactions with both EF-Tu and the ribosome[40]. Also, the sarcin-ricin loop (SRL) has been shown to drive His<sup>84</sup> spontaneously into the correct conformation for GTPase activation[45]. These changes lead to a distortion of the 3' end of the aa-tRNA, disrupting its interactions with the switch 1 loop[37]. It has been suggested that this lowered interaction could cause the switch 1 loop to open up and by this lead to a conformation change in the switch 2 region which gives catalytic residue

His<sup>84</sup> access to GTP. His<sup>84</sup> has been suggested to catalyse GTP hydrolysis by forming hydrogen bonds to water and/or the  $\gamma$ -phosphate. It has been shown that His<sup>84</sup> can not act as a general base and has to be protonated, explaining the pH dependence of hydrolysis [45]. The conformations of the switch 1 and 2 loops during hydrolysis are stabilized by interactions with the sarcin-ricin loop (SRL) of 23S rRNA[35]. Phosphate release is followed by large scale conformational changes of EF-Tu and tRNA accommodation. Recent findings show that EF-Tu's presence drives the aa-tRNA into a partially accommodated intermediate (elbow-accommodated) state, with its dynamics increasing the rate further[30]. Crystal structures of EF-Tu containing GDP show that domain 1 of EF-Tu rotates against against domains 2 and 3 by around  $100\text{\AA}^\circ$  compared to a GTP state. This motion has been suggested to cause EF-Tu release from the aa-tRNA and the ribosome, as it would disrupt the interactions between domain 1 and the SRL as well as the switch 2's interaction with the 3' end of the aa-tRNA[37].

### 1.1.5 Kirromycin

Kirromycin ( $\text{C}_{43}\text{H}_{60}\text{N}_2\text{O}_{12}$ ) is an antibiotic that binds to EF-Tu between domains 1 and 3 (see figure 1.5). Its structure consists of a 2-, 5-substituted 3-4 dihydroxytetrahydrofuran ring, a pyridone ring system, and a goldinoic acid, connected via two series of double conjugated bonds (see [27]). It has a very narrow antibacterial spectrum[48] limited by membrane selectivity, showing little to no effect on *Escherichia Coli* cells while inhibiting protein synthesis heavily in cell extract. Kirromycin binds to EF-Tu on residues 120, 124, 160, 316 and 375[1][28]. In the presence of kirromycin binding of the ternary complex to the ribosome is not inhibited, and GTP hydrolysis rates are increased. After hydrolysis however EF-Tu is not released from the ribosome, blocking peptide-bond formation as the aa-tRNA can not fully accommodate. As GTP hydrolysis is a non reversible step, the ternary complex can not dissociate from the ribosome either, halting protein synthesis on the affected ribosome completely. Kirromycin functions by preventing the conformational change of EF-Tu from its GTP to the GDP state[31]. The mechanism of how it prevents this change is not fully understood.



# 2 Methods

## 2.1 Molecular Dynamics Simulations

Molecular dynamics (MD) simulations are a tool to study molecular systems on an atomistic length scale, and femto- to millisecond timescale[21]. These timescales allow kirromycin's effect on the dynamics of EF-Tu to be studied on timescales experimentally not accessible. Crystallography can achieve time resolution of 150 ps[38], but this requires the process to be able to occur in crystalline state and also that it is possible to trigger this process after crystallization. Cryo-EM can also resolve structures time-wise, however the shortest dead-time between sample preparation and freezing is on the order of 1-10 milliseconds[14]. Short lived intermediate states occurring during this time can currently only be observed by MD simulations. To be able to access these timescales, in an MD simulation Newton's equations of motion are solved numerically for the system repeatedly.

### 2.1.1 Equations of motion

A system of atoms is completely described by the time-dependent Schrödinger equation:

$$i\hbar\frac{\partial}{\partial t}\Psi(\underline{r}; \underline{R}) = H \cdot \Psi(\underline{r}; \underline{R}) \quad (2.1)$$

with electron positions  $\underline{r}$  and nuclei positions  $\underline{R}$ . This equation is not analytically solvable for systems larger than  $H_2^+$ , and computationally too expensive to integrate, as the wave function would have to be integrated for every point in the definition space. Therefore, in order to study protein dynamics, approximations and assumptions have to be made:

- The electrons motion is fast compared to the nuclei motion, so that for the motion of the nuclei the electrons are in ground state configuration. This allows

## 2 Methods

the separate calculation of electron and nuclei motion (*Born-Oppenheimer* approximation),

- the nuclei motion can be described classically, and
- the groundstate energy of the electrons can be described by a force field, composed of multiple empirical functions.

### **Born-Oppenheimer approximation**

The Born-Oppenheimer approximation assumes that the electron's motion is fast enough compared to the motion of the nuclei, so that the electrons can be thought of as instantaneously relaxing into the ground-state for the given nuclei positions. Then the electrons ground-state energies can be calculated at fixed nuclei positions as a solution to the time-independent Schrödinger equation. This allows the wave function  $\Psi(\underline{r}, \underline{R})$  to be written as a product of the wave functions of electrons  $\psi_e(\underline{r}; \underline{R})$ , which is a wave function of the  $\underline{r}$  with the  $\underline{R}$  only as parameter, and nuclei  $\psi_n(\underline{R})$ (see [11]):

$$\Psi(\underline{r}, \underline{R}) = \psi_e(\underline{r}; \underline{R}) \cdot \psi_n(\underline{R}). \quad (2.2)$$

Given this product, the Schrödinger equation can be separated into two parts, one for each wave function:

$$H_e(\underline{r}; \underline{R})\psi_e(\underline{r}; \underline{R}) = E_e(\underline{R})\psi_e(\underline{r}; \underline{R}) \quad (2.3)$$

$$i\hbar \frac{\partial}{\partial t} \psi_n(\underline{R}) = (T_n + E_e(\underline{R}))\psi_n(\underline{R}), \quad (2.4)$$

where  $E_e(\underline{R})$  is the ground-state energy of the electrons for given nuclei positions. Eq. 2.3 can not be solved numerically in reasonable time for proteins since the amount of electrons and as such the search space for the minimum of energy is too large. Equation 2.4 can not be numerically solved in sufficient time either, because it still requires integrating the wave function on the whole phase space. Therefore further simplifications are necessary.

### **Classical mechanics for motion of nuclei**

A quantum mechanical description for the nuclei (eq. 2.4) is not feasible. An ad hoc solution is to describe the nuclei motion classically, replacing the time-dependent

Schrödinger equation with Newtons law of motion. For each nucleus  $i$  with mass  $m_i$  and position vector  $R_i$  we then have to solve

$$m_i \frac{d^2}{dt^2} R_i = F_i = -\nabla_i E_e(R_1, \dots, R_N),$$

where  $E_e$  is the groundstate energy of the electrons.

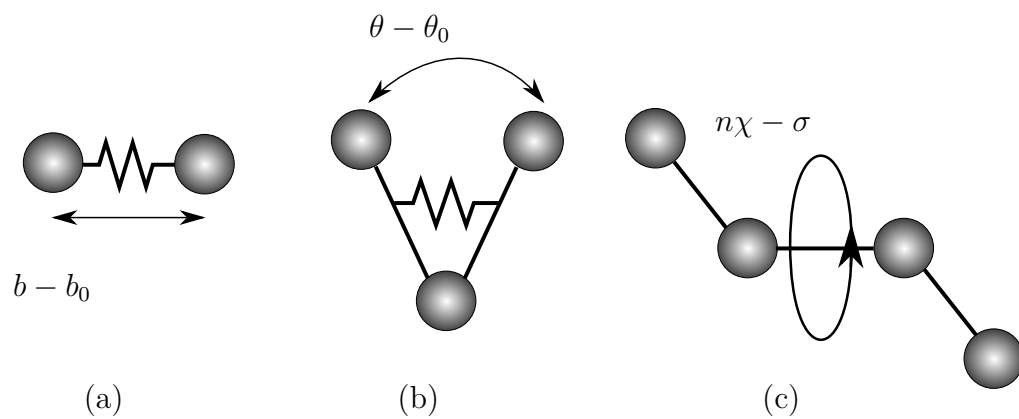
## Force Field

The groundstate energy  $E_e$  of the electrons required in equation 2.5 is computationally very expensive to calculate for proteins. Instead a force field  $V_e$  is used to describe the interactions. The force field is derived empirically[17] as a sum of bonded  $V_{bonded}$  and non-bonded  $V_{nonbonded}$  interactions (see figure 2.1) and a term  $V_{other}$ , which denotes force field specific corrections:

$$\begin{aligned} V_e &= V_{bonded} + V_{nonbonded} + V_{other} \\ V_{bonded} &= \sum_{bonds} K_b(b - b_0)^2 + \sum_{angles} K_\theta(\theta - \theta_0)^2 + \sum_{dihedrals} K_\chi(1 + \cos(n\chi - \sigma)) \\ V_{nonbonded} &= \sum_{nonbonded\ pairs\ ij} \left( \epsilon_{ij} \left[ \left( \frac{R_{min,ij}}{r_{ij}} \right)^{12} - 2 \cdot \left( \frac{R_{min,ij}}{r_{ij}} \right)^6 \right] + \frac{q_i q_j}{r_{ij}} \right) \end{aligned}$$

The first term of  $V_{bonded}$  is the potential used to model direct (i.e. chemical) bonds between two atoms A and B (also called 1,2 interactions). This model is a harmonic potential with distance between the centers of A and B  $b$ , a minimum at  $b_0$  and spring constant  $K_b$ , both of which are defined by the types of the two atoms involved and derived from experiments and quantum chemical calculations (see [32]). The second term describes the contribution from triplets, A bound to B and B bound to C.  $\theta$  is the angle between A and C (see figure 2.1 (b)), the potential is also harmonic, with a minimum at  $\theta_0$  and a spring constant  $K_\theta$ . In the last term the interaction between 4 atoms, where A is bound to B, B bound to C, and C bound to D, are described by their dihedral angle  $\chi$ . The dihedral formed by these atoms is periodic in  $\chi$ , a cosine is used to describe it.  $\sigma$  describes the position in which the energy is maximized,  $K_\chi$  scales the potential. The 1 is added so that the energy is always non-negative.

The non-bonded interactions are not calculated for pairs of atoms interacting in either 1,2 or 1,3 interactions. As the potentials are already modeled to fit spectroscopic and quantum-mechanical data, i.e. bond lengths and angles, they are



bonded interactions



non-bonded interactions

Figure 2.1: Types of interactions included in force fields. (a) represents bond, (b) angle, and (c) dihedral interactions. (d) is the coulomb interaction and (e) the Pauli repulsion and Van-der-Waals forces

sufficient. Adding non-bonded interactions to them would require changing the parameters of the bonded interactions to compensate, so that including them would not improve accuracy. With 1,4 interactions the non-bonded terms are calculated with adjusted parameters (see [32]). For the non-bonded interaction of atoms  $i$  and  $j$  in a distance of  $r_{ij}$  a Lennard Jones potential with a minimum at  $R_{min,ij}$  and a minimum of the energy  $\epsilon_{ij}$  is used to approximate van der Wals interactions and the Pauli repulsion.

Furthermore, Coulomb interactions for the partial charges of the atoms  $q_i$  and  $q_j$  are added. Since the number of non-bonded atom pairs is far larger than bonded pairs, calculation of  $V_{nonbonded}$  makes up most of the computational effort. Therefore, the short range Lennard-Jones term usually is only calculated for atoms within a certain cut off distance.

### 2.1.2 Integration of Newton equations for the nuclei

In this work integration is done with the Verlet-Algorithm([43]) as it is implemented in GROMACS 5.1, a program package designed for MD simulation and analysis of biophysical systems[4] which was used for all simulations in this work.

The Verlet-Algorithm uses forces  $F(t)$  and velocities  $v(t)$  to calculate the velocities at time  $t + \frac{\Delta t}{2}$ , where  $\Delta t$  is the timestep used:

$$v(t + \frac{\Delta t}{2}) = v(t) + \frac{\Delta t}{2m} F(t).$$

This velocity is then used to update positions  $R(t)$  and velocities at time  $t + \Delta t$ :

$$R(t + \Delta t) = R(t) + \Delta t \cdot v(t + \frac{\Delta t}{2})$$

$$v(t + \Delta t) = v(t + \frac{\Delta t}{2}) + \frac{\Delta t}{2m} F(t + \Delta t)$$

### Thermodynamic ensemble

The natural ensemble for a cell is at constant pressure and constant temperature. Single water molecules being inserted or removed from the simulation box will not have an impact on the protein dynamics, and a single copy of the ribosomal complex or EF-Tu will be simulated. Therefore constant particle numbers are used and the simulation will use an isothermic-isobaric ensemble (NPT). As the Verlet inte-

gration is symplectic, the energy drift experienced in numeric integration is small compared to non-symplectic integrators (e.g. Runge-Kutta)[15]. These small errors still have to be dealt with. Therefore all velocities are scaled by Berendsen Temperature coupling[8] each integration step, dependent on target temperature  $T_0$ , current temperature  $T$ , time step  $\Delta t$ , and coupling constant  $\tau_T$ .

$$\lambda = \sqrt{1 + \frac{\Delta t}{\tau_T} \left( \frac{T_0}{T} - 1 \right)} \quad (2.5)$$

$$v_{scaled} = v \cdot \lambda \quad (2.6)$$

Additionally, to achieve a constant pressure, Berendsen pressure coupling[8] is used. It scales the simulation box size and the positions of all atoms by a factor  $\mu$ , which depends linearly on the target pressure  $P_0$ , current pressure  $P$  (see [42]), and coupling time constant  $\tau_P$  and isothermal compressibility  $\kappa$

$$\mu = 1 - \frac{\Delta t}{\tau_P} \kappa (P_0 - P). \quad (2.7)$$

## 2.2 Secondary Structure Analysis

The secondary structure of EF-Tu's switch 1 loop is important for its function and can change during dynamics. To determine the secondary structure from our simulations, here we have used the DSSP (*Define Secondary Structure of Proteins*) algorithm[20] as implemented in GROMACS 5.1, which assigns 8 different structures. DSSP determines if the CO group of amino acid  $i$  and the NH group of amino acid  $j$  form a hydrogen bond by calculating the electrostatic interaction  $E$  with assumed partial charges of  $-0.42e$  and  $0.2e$ , respectively,

$$E = 0.084 \cdot \left( \frac{1}{r(O_i N_j)} + \frac{1}{r(C_i H_j)} - \frac{1}{r(O_i H_j)} - \frac{1}{r(C_i N_j)} \right) \cdot 332 \frac{\text{kcal}}{\text{mol}}, \quad (2.8)$$

with  $r(O_i N_j)$  being the distance between the two atoms. Is  $E$  below  $-0.5 \frac{\text{kcal}}{\text{mol}}$ , the hydrogen-bond is considered to be formed. The patterns of formed bonds and the angles between carbon atoms are then used to determine the secondary structure, some of which are displayed in figure 2.2.

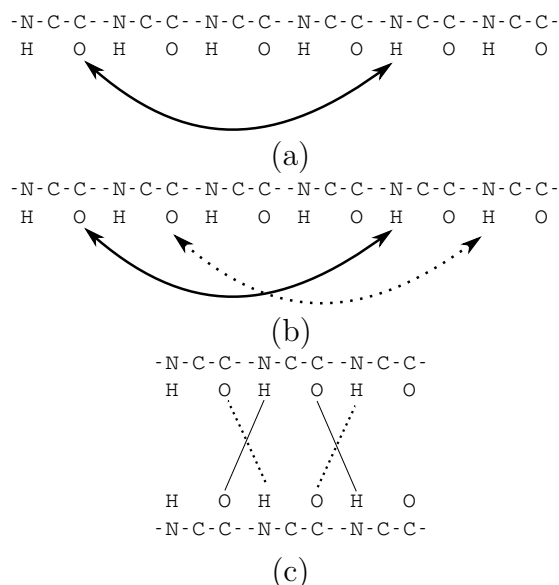


Figure 2.2: Three of the patterns used to distinguish secondary structure in the DSSP algorithm. (a) shows a 4-turn, (b) an  $\alpha$ -helix which consists of consecutive 4-turns, and (c) shows a parallel  $\beta$ -bridge which is one of two basic structures a  $\beta$ -sheet can consist of.  $\beta$ -sheets are formed by (anti)parallel  $\beta$ -bridges that are connected by a shared residue. Figure taken from [20].

## 2.3 Root Mean Square Deviation

The conformation changes EF-Tu undergoes are large and complex. To monitor these changes relative to experimental structures, root mean square deviation (RMSD) was used. To calculate it, both structures are first fitted onto a reference structure. The (mass-weighted) RMSD is then calculated as

$$RMSD = \sqrt{\frac{1}{\sum_i m_i} \frac{\sum_i m_i \cdot (\vec{x}_{i,1} - \vec{x}_{i,2})^2}{N}}, \quad (2.9)$$

where  $i$  goes over all atoms.

## 2.4 Principal Component Analysis

To determine whether kirromycin affects the functional motions of EF-Tu in a GT-Pase activated state, we want to identify these motions in the trajectories. Doing this by visually inspecting the trajectories is often difficult, because MD trajectories also contains high-frequency thermal vibrations which obscure the functional mo-

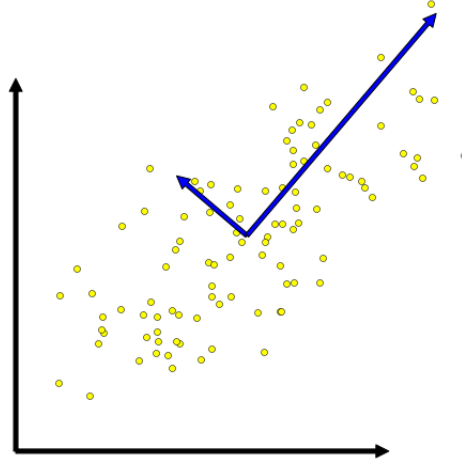


Figure 2.3: A data set with two bases, in black the base in which the data was generated, and in blue the base constructed by a PCA with vectors scaled according to the variance of the data along them.

tions. Functional motions are often large-scale, collective motions of the atoms of the protein. Therefore we separate the trajectory into linear, collective motions that describe as large as possible parts of the atom movement, i.e. maximize the variance along them. These motions are called principal moments. This process is sketched in figure 2.3. Principal moments are obtained by solving the eigenvalue problem of the covariance matrix<sup>[4]</sup>  $\Sigma$  of the vector  $R$  containing all atomic coordinates, with the entries

$$\Sigma_{ij} = \text{COV}(R_i, R_j) = \langle R_i \cdot R_j \rangle - \langle R_i \rangle \langle R_j \rangle . \quad (2.10)$$

Since this matrix is symmetric, square, and positive-semidefinite, it can always be transformed into a diagonal matrix:

$$X^T \Sigma X = \begin{pmatrix} \lambda_1 & 0 & 0 & \dots \\ 0 & \lambda_2 & 0 & \dots \\ \dots & & & \end{pmatrix} \quad (2.11)$$

where  $X$  is a matrix composed of the eigenvectors of  $\Sigma$ , and  $\lambda_i$  the eigenvalue corresponding to the  $i$ th eigenvector. This yields not only the largest variance principal moment, but also all others. The eigenvectors of  $\Sigma$  are the principal moments, their corresponding eigenvalue the variance along them. Transforming

```

simu 1  SKEKFERTKPHVNVGTIGHVDHGKTTLTAAITTVLAKTYGGAARAFDQIDNAPEEKARGITINTSHVEYDTPTRHYAHVD 80
lob2 1  AKEKFERTKPHVNVGTIGHVDHGKTTLTAAITTVLAKTYGGAARAFDQIDNAPEEKARGITINTSHVEYDTPTRHYAHVD 80
1dg1 1  KPHVNVGTIGHVDHGKTTLTAAITTVLAKTYGGAARAFDQIDNAPEEKARGITINTSHVEYDTPTRHYAHVDCPGHADYV 80
4v5q 1  AKGEFVRTKPHVNVGTIGHVDHGKTTLTAALTYVAAAENPNVINTAHVEYETAKRHYSHVDCPGHADYIKNMITGAAQMD 80

simu 1  SKEKFERTKPHVNVGTIGHVDHGKTTLTAAITTVLAKTYGGAARAFDQIDNAPEEKARGITINTSHVEYDTPTRHYAHVD 80
lob2 1  AKEKFERTKPHVNVGTIGHVDHGKTTLTAAITTVLAKTYGGAARAFDQIDNAPEEKARGITINTSHVEYDTPTRHYAHVD 80
1dg1 1  -----KPHVNVGTIGHVDHGKTTLTAAITTVLAKTYGGAARAFDQIDNAPEEKARGITINTSHVEYDTPTRHYAHVD 72
4v5q 1  AKGEFVRTKPHVNVGTIGHVDHGKTTLTAALTYVAAAENPNV-----INTAHVEYETAKRHYSHVD 61

```

Figure 2.4: Sequence alignment for the first amino acids of EF-Tu. Second and last column are the first and last amino acid of the structure shown respectively. On the top are the unaligned structures displayed in FASTA coding. The bottom shows the alignment with regions of high conservation in red. The first row is the structure used for simulation, the other rows are crystal structures.

the data into this basis yields the principal components  $\underline{P}$ :

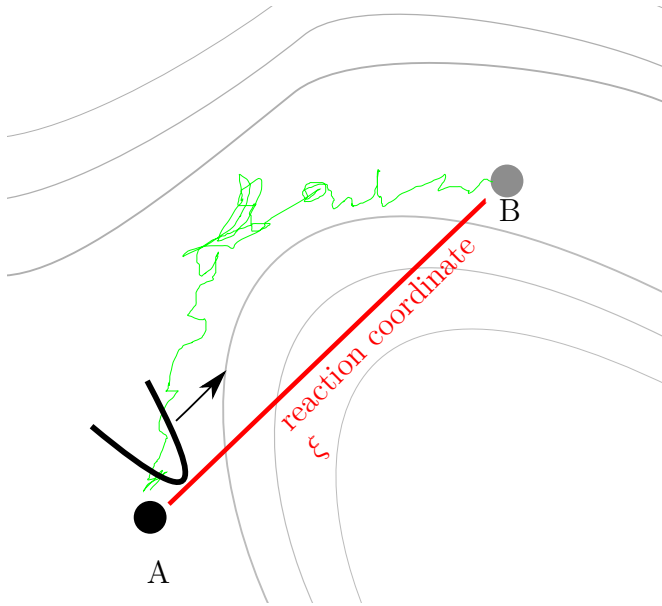
$$\underline{P} = X^t \cdot (R - \langle R \rangle). \quad (2.12)$$

## 2.5 Sequence Alignment

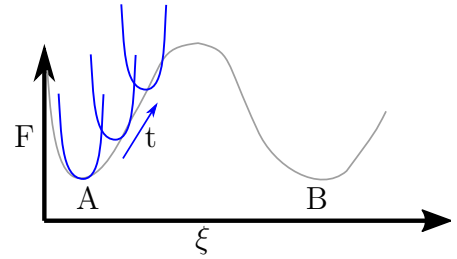
Although EF-Tu is highly conserved across species, its amino acid sequence is not exactly the same in all of them. Further, experimental structures sometimes are lacking parts of the molecule because they were not resolved well. To compare structures with a PCA it is necessary that they only contain matching atoms. Comparing the MD simulations to experimental structures therefore requires that residues missing in one of the structures are removed from the other structures until the biggest common structure remains. Mismatching side groups have been ignored as only the backbone of the amino acids was used for the PCA. Finding the amino acids that need to be removed is done by aligning the sequences. Here, BLASTs[5] protein alignment tool[6] has been used to this goal. Part of such a result is shown in figure 2.4. If any of the structures shows a gap (denoted by "-") at a position, the amino acids at this position are not taken into account for the PCA.

## 2.6 Umbrella sampling

The conformation of EF-Tu differs drastically between GTP and GDP state. The simulated EF-Tu<sub>crysto-EM</sub> · GDP complex is expected to change from the kirromycin



(a) Sketch of a possible umbrella sampling to calculate the free energy landscape between A and B. In red is the reaction coordinate along which a biasing potential is applied. Green shows a possible trajectory.



(b) Sketch of a free energy profile along the reaction coordinate. Shown in blue are the biasing potentials. The potential the system experiences is the sum of both free energy landscape and biasing potential. Moving the biasing potential can then be used to guide the system across free energy barriers.

induced GTP-like conformation to the GDP one. If this change is not observed, simulation time could either be too short, or the change could be obstructed by large free energy barriers. The existence of such barriers could, depending on the barrier height, indicate that this change occurs *in vivo* only efficiently in the ternary complex of EF-Tu, ribosome and tRNA. To calculate the free energy landscape between two structures, Umbrella sampling will be used here.

The free energy  $F$  can be calculated from the partition function  $Z$  as(compare [22])

$$F = -\frac{1}{\beta} \ln(Z), \quad (2.13)$$

with  $\beta = \frac{1}{k_B T}$  with Boltzmann constant  $k_B$  and temperature  $T$ . To calculate the free energy landscape along a reaction coordinate  $\xi$  (for example the difference vector between the two structures, see figure 2.5b), one therefore has to find a way to solve

$$Z(\xi) = \frac{\int \exp(-\beta E(x)) \delta(\xi(x) - \xi) d^N x}{\int \exp(-\beta E(x)) d^N x} \quad (2.14)$$

The partition function could be calculated from the simulated data directly if simulation times were infinite. As the systems are ergodic, the partition function

could be obtained by using the time-average of the simulation instead of integrating over the whole conformation space. With finite simulation times however, regions of phase space obstructed by a large energy barrier are often times not sampled at all, and regions with high energy sampled insufficiently to model the energy landscape. To still obtain the free energy landscape, a biasing potential is applied that guides the system into the undersampled regions. This potential is applied along the reaction coordinate which starts with its minimum at the start structure and slowly moves towards the desired end structure.

Retrieving the unbiased free energy difference from a biased partition function is achievable, since the bias term  $f(\xi)$  is purely additive :

$$E_{bias}(x) = E(x) + f(\xi) \quad (2.15)$$

So the biased partition function  $Z_{bias}(\xi)$  is simply

$$Z_{bias}(\xi) = \frac{\int \exp(-\beta(E(x) + f(\xi(x)))) \delta(\xi(x) - \xi) d^N x}{\int \exp(-\beta E(x) + f(\xi(x))) d^N x}, \quad (2.16)$$

and the unbiased  $Z(\xi)$  is simply (compare equations 2.16 and 2.14)

$$Z(\xi) = Z_{bias}(\xi) \cdot \exp(-\beta f(\xi)) \cdot \langle \exp(-\beta f(\xi)) \rangle_{\xi} \quad (2.17)$$

$$\Rightarrow F(\xi) = -k_B T (\ln(Z_{bias}(\xi)) + \ln(\langle \exp(-\beta f(\xi)) \rangle)) - f(\xi) \quad (2.18)$$

Since the error of the approximated landscape is inversely dependent on the sampling, from the guided trajectory several snapshots are taken and simulated with the bias potential at a fixed position. The snapshots are chosen such that their trajectories, when projected onto the reaction coordinate, overlap. These snapshots are then analysed with WHAM (see [25]).

Umbrella sampling hinges on choosing a suitable biasing potential. Imposing artificial restrictions on a system can lead to unphysiological conformation changes. Too few restrictions, and the system will not necessarily reach the intended conformation. The pulling coordinate chosen here is the difference vector of two structures in conformational space.

## 2.7 System Set-up

For all simulations the AMBER99SB (see [19]) force field has been used with the SPC/E[7] [9] water model. The target temperature for coupling is 300 K, and target pressure is 1 atm,  $\tau_T = 0.1$  ps and  $\tau_p = 1$  ps. A dodecahedral simulation box with periodic boundary conditions was used. An ionic concentrations of 7 mM magnesium chloride and 150 mM potassium chloride was reached by replacing water with the GROMACS program GENION, making sure the total charge of the system is zero. The cut-off range for the Lennard-Jones potential used was 1 nm. The simulations were carried out in 5 steps:

1. position restraints put on all atoms that are not part of the solvent and are not hydrogen
2. energy minimization, using steepest descent, the maximum accepted force was  $0.01 \frac{\text{J}}{\text{mol}\cdot\text{nm}}$ ,
3. simulated with position restraints in place for 50 ns,
4. release of the position restraints over 20 ns (force constant decreased linearly),
5. simulation time of 2  $\mu\text{s}$ .

Using these steps, overall ten 2  $\mu\text{s}$  long simulations of EF-Tu have been analysed.

### 2.7.1 Ribosomal simulations

Two simulations, each 2  $\mu\text{s}$  long, of the whole ribosome with EF-Tu on it have been analysed for this work. They have not been executed in the scope but been provided by Lars V. Bock (see [13]). The cryo-EM structures (PDB code 5AFI) are of the whole ribosome in complex with EF-Tu and kirromycin. As the switch 1 loop is very flexible and was badly resolved, for the simulations it has been modeled in using crystal structures of EF-Tu with tRNA and kirromycin in solution. For one of the simulations, kirromycin has been removed from the structure. The simulation times step used was 2 fs.

### 2.7.2 Free simulations

To start the free simulations from the cryo-EM structure, EF-Tu was cut out from the structure (with kirromycin). The same simulation protocol as before was used,

twice with and twice without kirromycin with a time step of 2 fs. Simulations started from the end of the ribosomal run were carried out with the same protocol, the starting configuration was simply cut out from the last frame. Simulations from the crystal structure *1dg1* [2] were done in the same way, one of the two EF-Tu's (protein H, the RMSD between the two structures is 0.19 nm) of the structure was chosen for simulation.



# 3 Results

## 3.1 Influence of Kirromycin on EF-Tu dynamics

During translation, tRNAs in complex with EF-Tu decode the mRNA codon. Before full tRNA accommodation, EF-Tu has to dissociate from the ribosome. The dissociation is preceded by GTP hydrolysis, followed by large conformational changes of EF-Tu[23]. Kirromycin has been suggested to prevent dissociation by keeping EF-Tu in a GTP-like conformation[31]. To investigate if the conformations and dynamics of EF-Tu are different when EF-Tu is in complex with the ribosome or in solution, and in presence or absence of kirromycin, we used a PCA to extract large scale conformation changes of EF-Tu in the simulations from trajectories. If the hypothesis is true, the simulations with kirromycin should show no conformational changes while the simulations without should develop towards the GDP conformation of EF-Tu. Further, because kirromycin binds between two domains it would be expected that it also affects the dynamics of EF-Tu with GDP alone in solution. To test this, we have performed and analysed simulations of EF-Tu with GDP in solution started from the conformation of the EF-Tu<sub>cryo-EM</sub> · GDP · Kir · Rib cryo-EM structure[13] with and without kirromycin as well as from a crystal structure of EF-Tu<sub>GDPcrystal</sub> · GDP [2].

### 3.1.1 Quaternary dynamics change of EF-Tu

First, we analysed the effect of kirromycin on the quaternary dynamics of EF-Tu by performing a PCA over the backbone atoms of EF-Tu, while also using the backbone to fit onto, from the simulation trajectories of the EF-Tu<sub>cryo-EM</sub> · GDP · Kir · Rib and EF-Tu<sub>cryo-EM</sub> · GDP · Rib complexes. The projections of the trajectories into the plane of the resulting first two eigenvectors is shown in figure 3.1 For simulations of the EF-Tu<sub>cryo-EM</sub> · GDP · Kir · Rib complex (red dots), the EF-Tu backbone conformation stays close the start structure (yellow symbol). A crystal structure (obtained from the PDB, code 1ob2) of the ternary EF-Tu · GNP · tRNA

### 3 Results

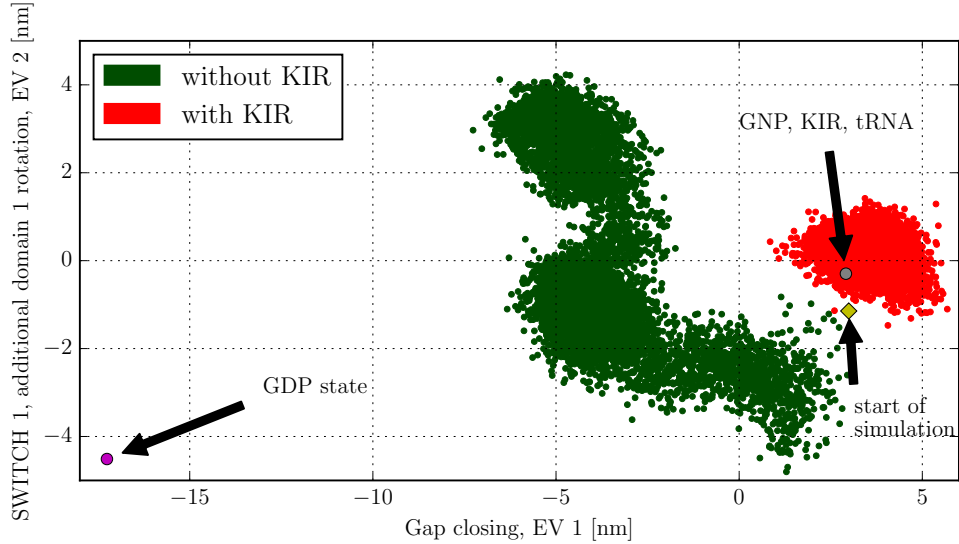


Figure 3.1: PCA of the trajectories of the EF-Tu backbone atoms obtained from  $\text{EF-Tu}_{\text{cryo-EM}} \cdot \text{GDP} \cdot \text{Rib}$  and  $\text{EF-Tu}_{\text{cryo-EM}} \cdot \text{GDP} \cdot \text{Kir} \cdot \text{Rib}$  complex simulations. The dots represent projections onto the first two eigenvectors for the simulations (green and red), the  $\text{EF-Tu}_{\text{cryo-EM}} \cdot \text{GDP} \cdot \text{Kir} \cdot \text{Rib}$  complex (yellow[13]), as well as  $\text{EF-Tu}_{\text{GDPcrystal}} \cdot \text{GDP}$  (magenta[2]) and  $\text{EF-Tu} \cdot \text{GNP} \cdot \text{tRNA}$  crystal structures (grey, PDB structure 1ob2, unpublished).

complex (grey symbol) falls directly into the explored phase-space region, with an RMSD of 0.28 nm of the  $\text{EF-Tu} \cdot \text{GNP} \cdot \text{tRNA}$  complex to the end structure of the  $\text{EF-Tu}_{\text{cryo-EM}} \cdot \text{GDP} \cdot \text{Kir} \cdot \text{Rib}$  complex simulation. GNP is an experimental substitution for GTP which can not hydrolyse and causes proteins to remain in GTP conformations. In the  $\text{EF-Tu}_{\text{cryo-EM}} \cdot \text{GDP} \cdot \text{Rib}$  complex simulations (green dots) EF-Tu moves away from the cryo-EM structure quickly. It moves in the direction of the conformation of a  $\text{EF-Tu}_{\text{GDPcrystal}} \cdot \text{GDP}$  crystal structure in the first eigenvector. The motion described by the first eigenvector, depicted in figure 3.2a, is a rotation of domain 1 against domain 3, which decreases the gap between the two subunits. The second eigenvector also describes a rotation of domain 1 against domain 3, in a plane orthogonal to the first eigenvector. In figure 3.2b the extremal representation of this motion is shown. The conformation change observed in the first eigenvector is unlikely to occur with kirromycin bound, as the binding sites of kirromycin move in a way that would require kirromycin to stretch. Kirromycin is however a rigid molecule. This indicates that kirromycin does inhibit EF-Tu’s dynamics, preventing a rotation of domain 1 towards domain 3 sterically.

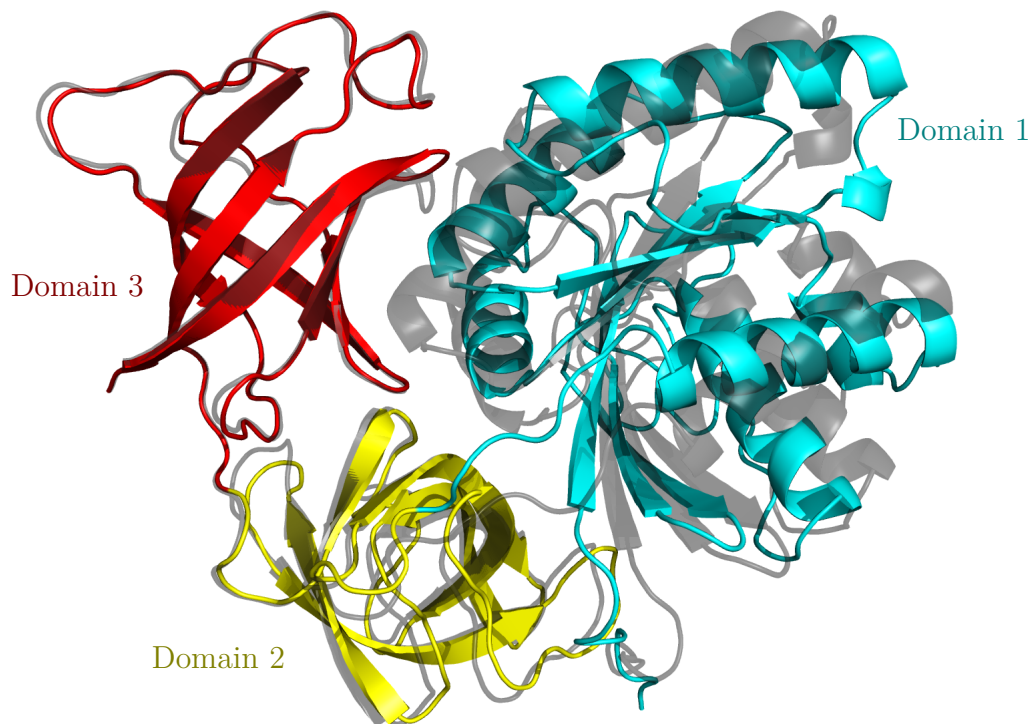
The conformation of EF-Tu did not reach the GDP state in the EF-Tu<sub>crysto-EM</sub> · GDP · Rib simulations. As the conformation change required to reach the GDP state is large, it may be inhibited by being attached to the ribosome and tRNA. Since simulations of EF-Tu in solution without the ribosome and without tRNA may exhibit different motions, another set of basis vectors obtained by PCA is necessary. The PCA was performed for the backbone of EF-Tu, over all simulations, now also including simulations of the EF-Tu<sub>crysto-EM</sub> · GDP , EF-Tu<sub>crysto-EM</sub> · GDP · Kir , and EF-Tu<sub>GDPcrystal</sub> · GDP complexes. Over 85% of variance is already contained in the first two eigenvectors (figure 3.4), so that the following analysis will be limited to them. The first eigenvector is dominated by the difference between the crystal and cryo-EM structure, mainly a rotation of domain 1 (figure 3.8). The second eigenvector contains the gap closing motion that was described previously. The resulting projection on the first two eigenvectors is in figure 3.3. EF-Tu<sub>crysto-EM</sub> · GDP complex simulations (cyan dots) sample a larger amount of conformation space than the EF-Tu<sub>crysto-EM</sub> · GDP · Kir simulations (orange).

The PCAs done over the backbone of EF-Tu from the simulations suggest that kirromycin inhibits the dynamics. Comparison of EF-Tu · GNP · tRNA crystal structure with the EF-Tu<sub>crysto-EM</sub> · GDP · Kir · Rib simulations indicates that EF-Tu stays in the GTP conformation.

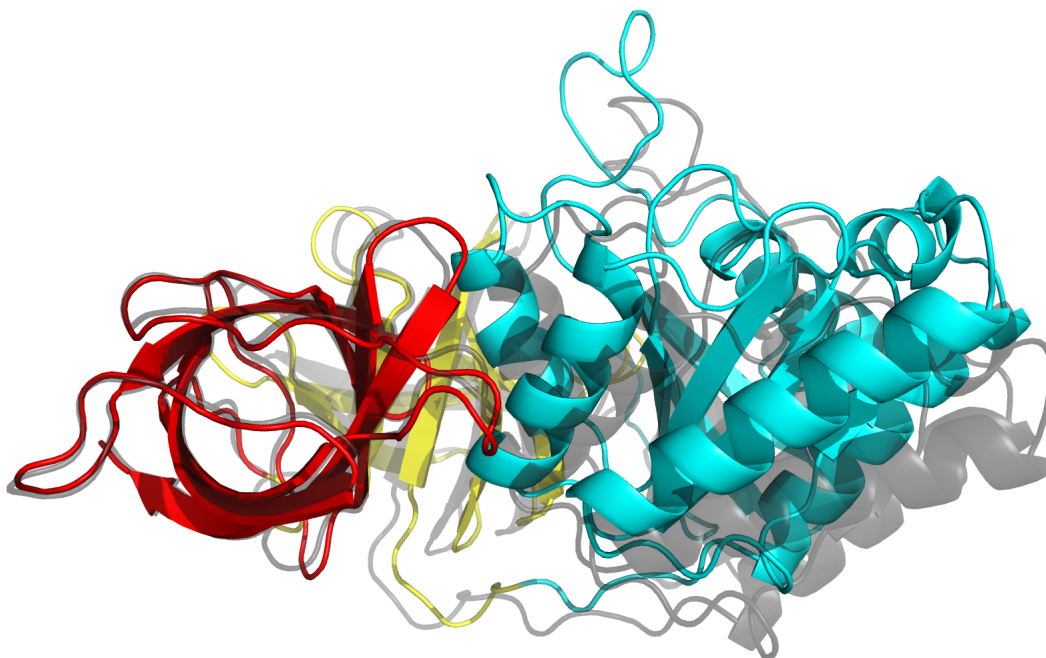
#### 3.1.2 Switch 1 secondary structure behaviour

The switch 1 loops secondary structure is thought to change from an  $\alpha$ -helical to a  $\beta$ -sheet conformation after GTP hydrolysis[2], because experimental structures of the GTP state in solution show the  $\alpha$ -helical conformation while the  $\beta$ -sheet structure is observed for GDP structures. This motion has been proposed to precede EF-Tu dissociation[2][44]. The first PCA eigenvector (see figure 3.1) of the EF-Tu<sub>crysto-EM</sub> · GDP · Rib and EF-Tu<sub>crysto-EM</sub> · GDP · Kir · Rib simulations contained, in addition to the gap closing, an opening of the  $\alpha$ -helical structures of switch 1. To further and more accurately study this change, the secondary structure was determined with the DSSP[20] analysis tool from the GROMACS 5.1[3] package.

The conformation of switch 1 in the course of each simulation type is depicted in figure 3.6, the end states are visualized in figure 3.5. Simulations on the ribosome with kirromycin exhibit the  $\alpha$ -helical conformation, where the switch 1 loop has two  $\alpha$  helices, from residue 46 to 50 and from 53 to 59. During the simulations of the EF-Tu<sub>crysto-EM</sub> · GDP · Kir · Rib complex these  $\alpha$ -helical structures persist through-



(a) Representation for eigenvector 1. The opaque structure represents the minimum, the transparent the maximum.



(b) Representation for eigenvector 2. The opaque structure represents the minimum, the transparent the maximum.

Figure 3.2: Two conformations corresponding to the extreme projections of the simulations onto the first two eigenvectors of the PCA of the EF-Tu backbone are shown in ribbon representation . EF-Tu is coloured according to its domains.

### 3.1 Influence of Kirromycin on EF-Tu dynamics

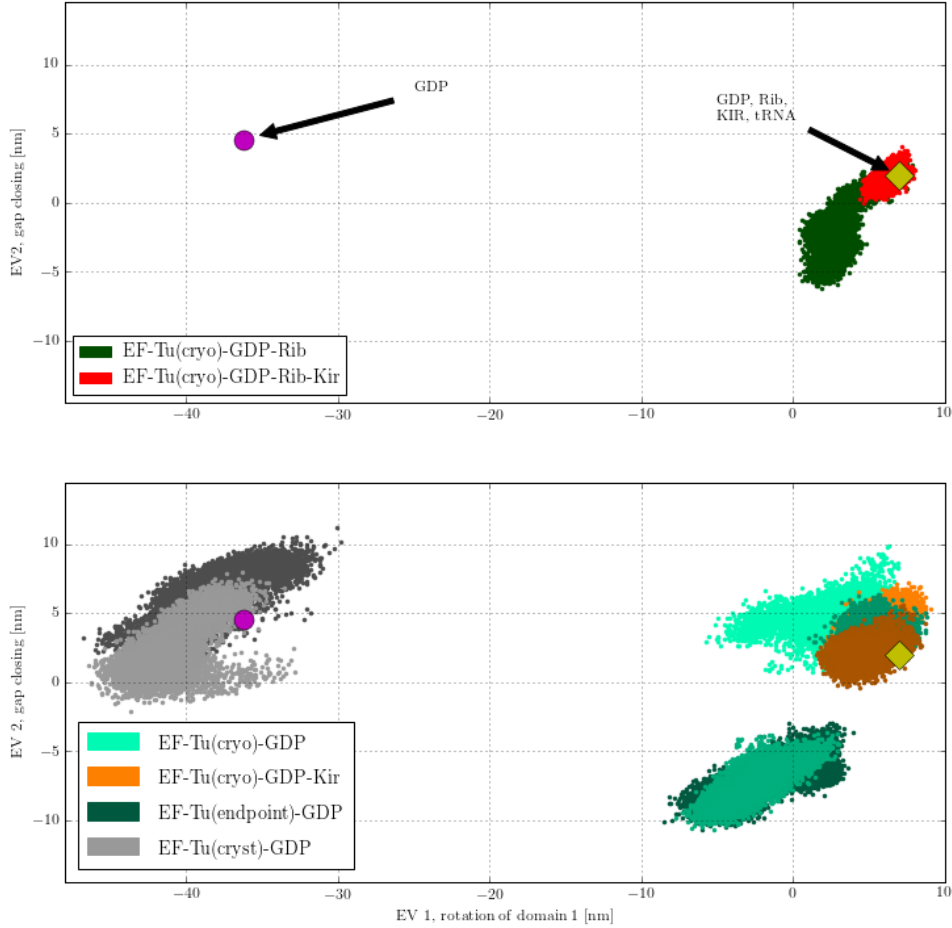


Figure 3.3: PCA of the trajectories of the EF-Tu backbone atoms obtained from simulations of EF-Tu in complex with the ribosome and in solution. The dots represent projections onto the first two eigenvectors for the ribosome simulations (green and red), simulations in solution with kirromycin (orange) and without (bright cyan  $\text{EF-Tu}_{\text{cryo-EM}} \cdot \text{GDP} \cdot \text{Rib}$ , dark cyan from the endpoint and grey for simulations started from  $\text{EF-Tu}_{\text{GDPcrystal}} \cdot \text{GDP}$  structure), the  $\text{EF-Tu}_{\text{cryo-EM}} \cdot \text{GDP} \cdot \text{Kir} \cdot \text{Rib}$  structure (yellow[13]), as well as  $\text{EF-Tu}_{\text{GDPcrystal}} \cdot \text{GDP}$  (magenta[2])

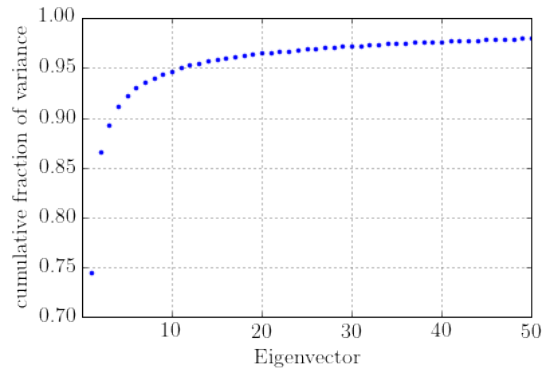


Figure 3.4: Cumulative variance along the eigenvectors. The eigenvectors have been sorted according to the size of the variance along them, shown are only the first 50.

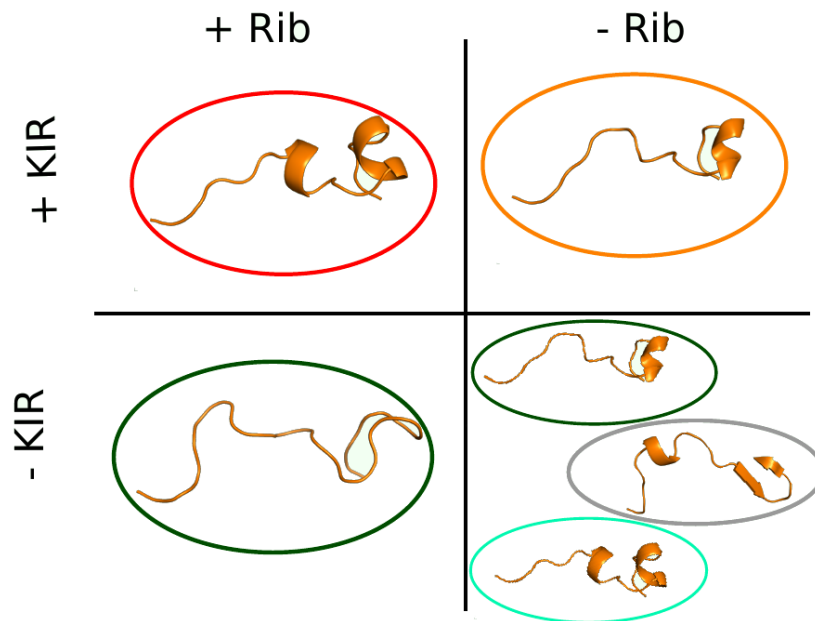


Figure 3.5: Different secondary structure conformations of the switch 1 loop for different simulation conditions and starting conformations. The structures are encircled by the colours used in 3.3, red for  $\text{EF-Tu}_{\text{cryo-EM}} \cdot \text{GDP} \cdot \text{Kir} \cdot \text{Rib}$  and dark green for  $\text{EF-Tu}_{\text{cryo-EM}} \cdot \text{GDP} \cdot \text{Rib}$ , orange for  $\text{EF-Tu}_{\text{cryo-EM}} \cdot \text{GDP} \cdot \text{Kir}$ , cyan for  $\text{EF-Tu}_{\text{cryo-EM}} \cdot \text{GDP}$ , green for  $\text{EF-Tu}_{\text{endpoint}} \cdot \text{GDP}$  and grey for  $\text{EF-Tu}_{\text{GDPcrystal}} \cdot \text{GDP}$ .

out the simulation as expected (figure 3.6a). Without kirromycin, the first, small helix unfolded already during the release of the position restraints, the second helix unfolds roughly  $1.5 \mu\text{s}$  after the simulation start and  $1.2 \mu\text{s}$  after gap closing. As helix opening occurs after gap closing and not in the EF-Tu<sub>cryo-EM</sub> · GDP · Kir · Rib complex simulations, where the gap closing is not observed, these motions might be related. Further, this opening of the helices is necessary to reach the  $\beta$ -sheet conformation of switch 1, which is present in the EF-Tu<sub>GDPcrystal</sub> · GDP crystal structure of EF-Tu.

In the simulations of the EF-Tu<sub>cryo-EM</sub> · GDP complex, the secondary structure remains in the  $\alpha$ -helical conformation. For the EF-Tu<sub>endpoint</sub> · GDP simulations, which started with both helices opened, the second helix closes. This indicates that lowered interaction energies with the tRNA alone can not be responsible for unwinding in EF-Tu<sub>cryo-EM</sub> · GDP · Rib simulations and that the opening of the second helix is facilitated by the ribosome and tRNA.

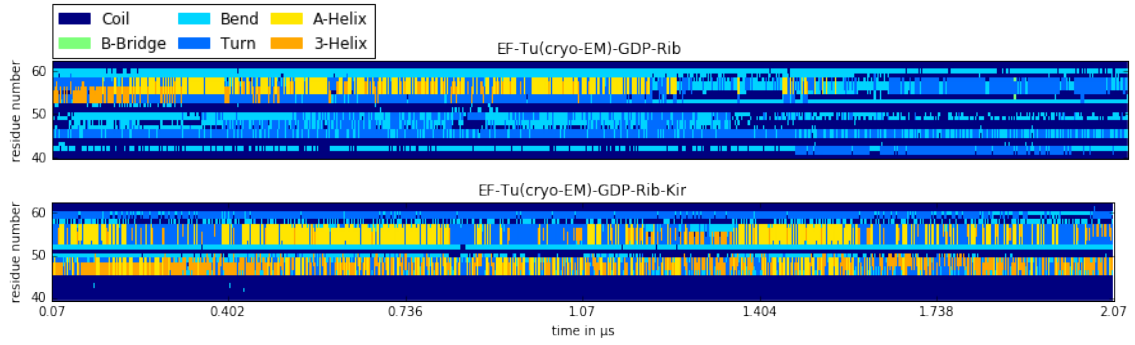
The second helix remained in  $\beta$ -sheet conformation for the EF-Tu<sub>GDPcrystal</sub> · GDP simulations, which is the same as in the crystal structure[2].

It has also been proposed that the switch 1 has a disordered structure before GTP hydrolysis, which opens the hydrophobic gate[44][37]. If the switch 1 becomes disordered before GTP hydrolysis *in vivo*, it would be expected that in the simulations of the EF-Tu<sub>cryo-EM</sub> · GDP · Kir · Rib complex the switch 1 loop also becomes disordered, as it is a complex with GDP. The DSSP results in figure 3.6a however show that the secondary structure remains  $\alpha$ -helical. A disordered secondary structure was proposed because of the expected high mobility of such a structure, which could explain the low electron densities observed in experiments for the switch 1 loop[44]. However, the switch 1 loop is very mobile in the EF-Tu<sub>cryo-EM</sub> · GDP · Kir · Rib complex simulations, compared to most other parts of EF-Tu's domain 1 (figure 3.7), even with switch 1's  $\alpha$ -helical structure. Therefore, low electron densities do not necessarily suggest a disordered structure, rather this would indicate that a secondary structure change of the switch 1 loop is not necessary for hydrolysis.

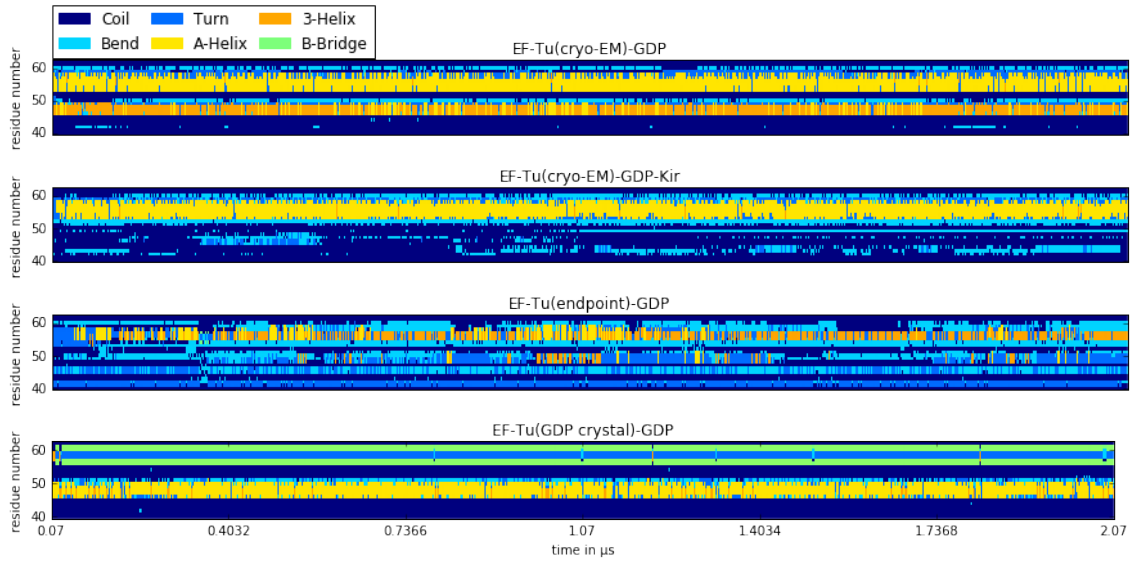
#### 3.1.3 Validity of switch 1 structure

The switch 1 loop was not resolved in the cryo-EM structure of the EF-Tu<sub>cryo-EM</sub> · GDP · Kir · Rib complex. As such it had to be modeled in for the simulations, which was done by Lars V. Bock. The structure of the loop was taken from the crystal structure with PDB code 1ob2 (unpublished), a structure of the complex of

### 3 Results



(a) DSSP analysis for simulations of the ribosomal complex.



(b) DSSP analysis for simulations of free EF-Tu.

Figure 3.6: DSSP analysis of the trajectories of the switch 1’s backbone. The colours show the secondary structure that was assigned to each residue of the loop at a given time. Blue colours represent turns and coils, orange colours represent helices and green colours  $\beta$ -sheets and bridges.

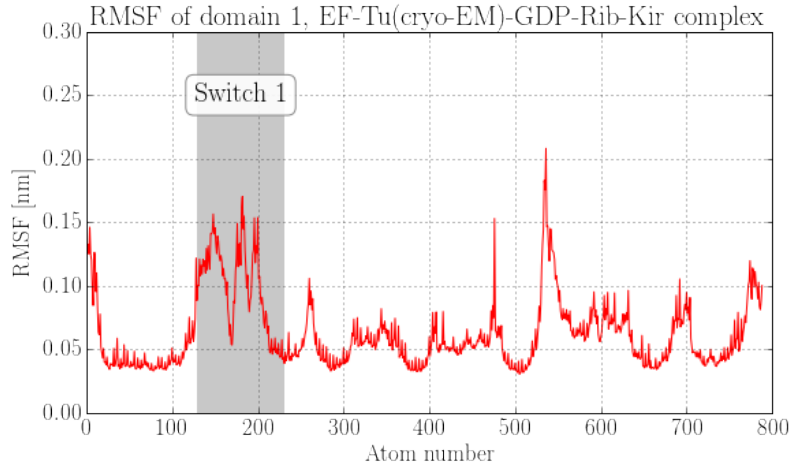


Figure 3.7: RMSF for each backbone atom of domain 1 for the simulation of the  $\text{EF-Tu}_{\text{cryo-EM}} \cdot \text{GDP} \cdot \text{Kir} \cdot \text{Rib}$  complex. Highlighted is the switch 1 region.

$\text{EF-Tu} \cdot \text{GNP} \cdot \text{tRNA}$ . During the  $\text{EF-Tu}_{\text{cryo-EM}} \cdot \text{GDP} \cdot \text{Kir} \cdot \text{Rib}$  simulation switch 1's secondary structure is stable (see figure 3.6), and the GTP crystal structure lies inside the explored phase space (figure 3.1). This indicates that the model is valid on the simulated timescales.

## 3.2 Kirromycin-free EF-Tu dynamics

As kirromycin is thought to keep EF-Tu in a GTP conformation[31], while not preventing hydrolysis of GTP to GDP, it is expected that removing kirromycin from the  $\text{EF-Tu}_{\text{cryo-EM}} \cdot \text{GDP} \cdot \text{Kir} \cdot \text{Rib}$  structure should lead to EF-Tu assuming its GDP conformation. To test this, the simulations without kirromycin are compared to simulations started from a GDP crystal structure[2], using the PCA basis obtained from all simulations, seen in figure 3.3.

The gap closing between domains 1 and 3 observed in the simulation on the ribosome after removal of kirromycin is not observed in simulations started from the  $\text{EF-Tu}_{\text{cryo-EM}} \cdot \text{GDP}$  structure. Rather, the gap is widened, the simulations reach projections onto the second eigenvector similar to the  $\text{EF-Tu}_{\text{GDPcrystal}} \cdot \text{GDP}$  structure. With the simulations of the  $\text{EF-Tu}_{\text{endpoint}} \cdot \text{GDP}$  structure the RMSD between the simulation and the  $\text{EF-Tu}_{\text{GDPcrystal}} \cdot \text{GDP}$  structure decreases slightly from 1.05 nm at the endpoint of the ribosomal simulations to 0.93 nm. In the plane of the first two eigenvectors, neither the simulations of the ribosomal complex nor the free

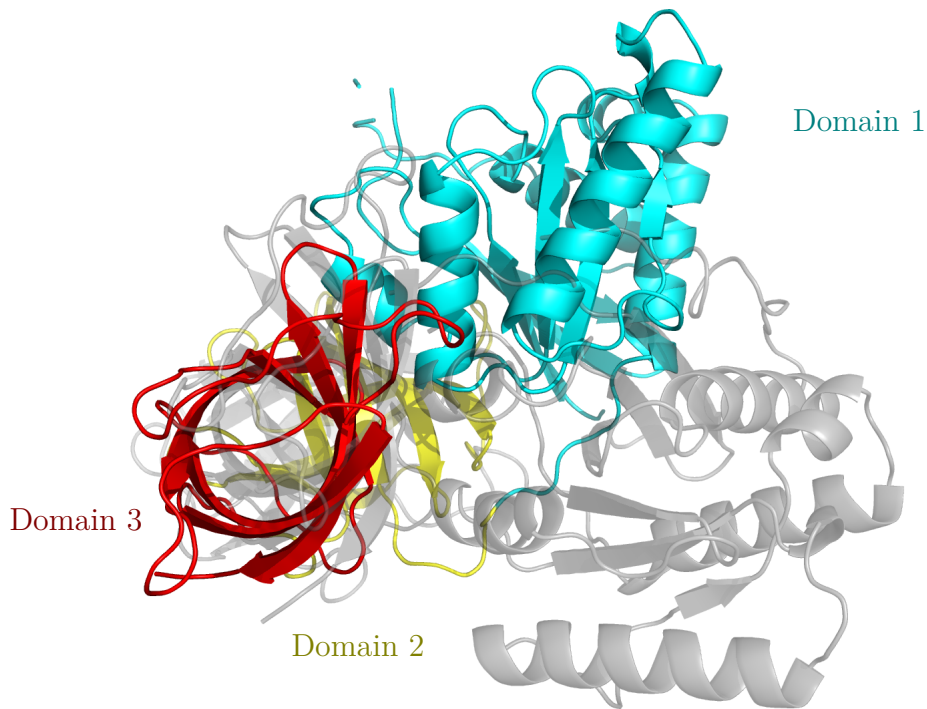


Figure 3.8: Two conformations representing the extremal values along the first eigenvector of the PCA based on all simulations are shown in ribbon representation. The grey translucent structure is close to the  $\text{EF-Tu}_{\text{GDPcrystal}} \cdot \text{GDP}$  conformation, the coloured structure close to the  $\text{EF-Tu}_{\text{cryo-EM}} \cdot \text{GDP} \cdot \text{Kir} \cdot \text{Rib}$  structure.. EF-Tu is coloured according to its domains.

simulations reach the GDP conformation. As can be seen in figure 3.8, which shows the extremal representation of the first eigenvector, the difference between GTP and GDP conformation is large. The timescale on which this change happens is not known, the simulation on the ribosome is likely not long enough for this conformation change to occur. The fact that this distance is not covered in the free simulations, could also be caused by the simulation times being too short. Or, since the simulations of the  $\text{EF-Tu}_{\text{cryo-EM}} \cdot \text{GDP}$  complex explore vastly different phase space when compared to the  $\text{EF-Tu}_{\text{cryo-EM}} \cdot \text{GDP} \cdot \text{Rib}$  simulations, the motion could be restricted by a free energy barrier that is not present for the ribosomal complex. This would further indicate that the ribosome is assisting in the conformational change. It has also been proposed that after GTP hydrolysis and phosphate release domain 1 of EF-Tu rotates outward on the ribosome, away from the tRNA and the sarcin-ricin loop of the EF-Tu binding pocket, which could reduce the binding en-

ergy and thus allow dissociation[37]. The proposed motion is similar to the motion described by the first eigenvector of the PCA (figure 3.8). However as only EF-Tu was taken into account in this analysis, the motion can not be related to the tRNA. To see if the observed motion is similar to the proposed, a PCA was done of the EF-Tu<sub>cryo-EM</sub> · GDP · Kir · Rib and EF-Tu<sub>cryo-EM</sub> · GDP · Rib simulations, which were fitted onto a shell of rRNA with a radius of 3.5 nm around EF-Tu. By filtering the trajectory to only contain the motions of the first two eigenvectors and visual inspection it was determined that the rotation contained in the second eigenvector is similar to the one observed before (figure 3.2b) , but it is not a rotation of domain 1 outwards with domains 2 and 3 still as was proposed.

### 3.2.1 Umbrella sampling

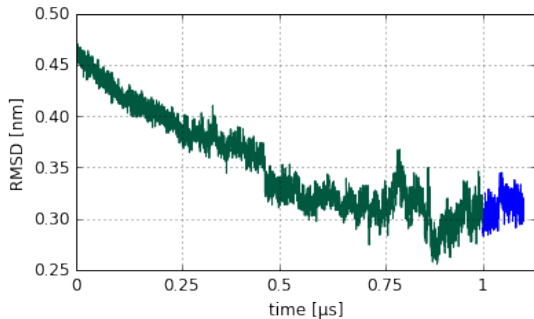


Figure 3.9: RMSD of the pulling simulation starting from the continuation run pulled towards a structure close to the cryo-EM structure. The green part is the pulling simulation, the blue part simulated from the end structure with turned off pulling potential.

As the difference between the EF-Tu<sub>GDPcrystal</sub> · GDP and EF-Tu<sub>cryo-EM</sub> · GDP complexes are too large to be overcome in free simulations in realistic time, artificial pulling forces had to be applied to EF-Tu. This was done between three structures, one taken from simulations started from the EF-Tu<sub>GDPcrystal</sub> · GDP , EF-Tu<sub>cryo-EM</sub> · GDP and EF-Tu<sub>endpoint</sub> · GDP structures each (see figure 3.10a). The cryo-EM and crystal structures were not used as target structures because the preparations necessary for imaging can fixate a protein in an unphysical conformation.

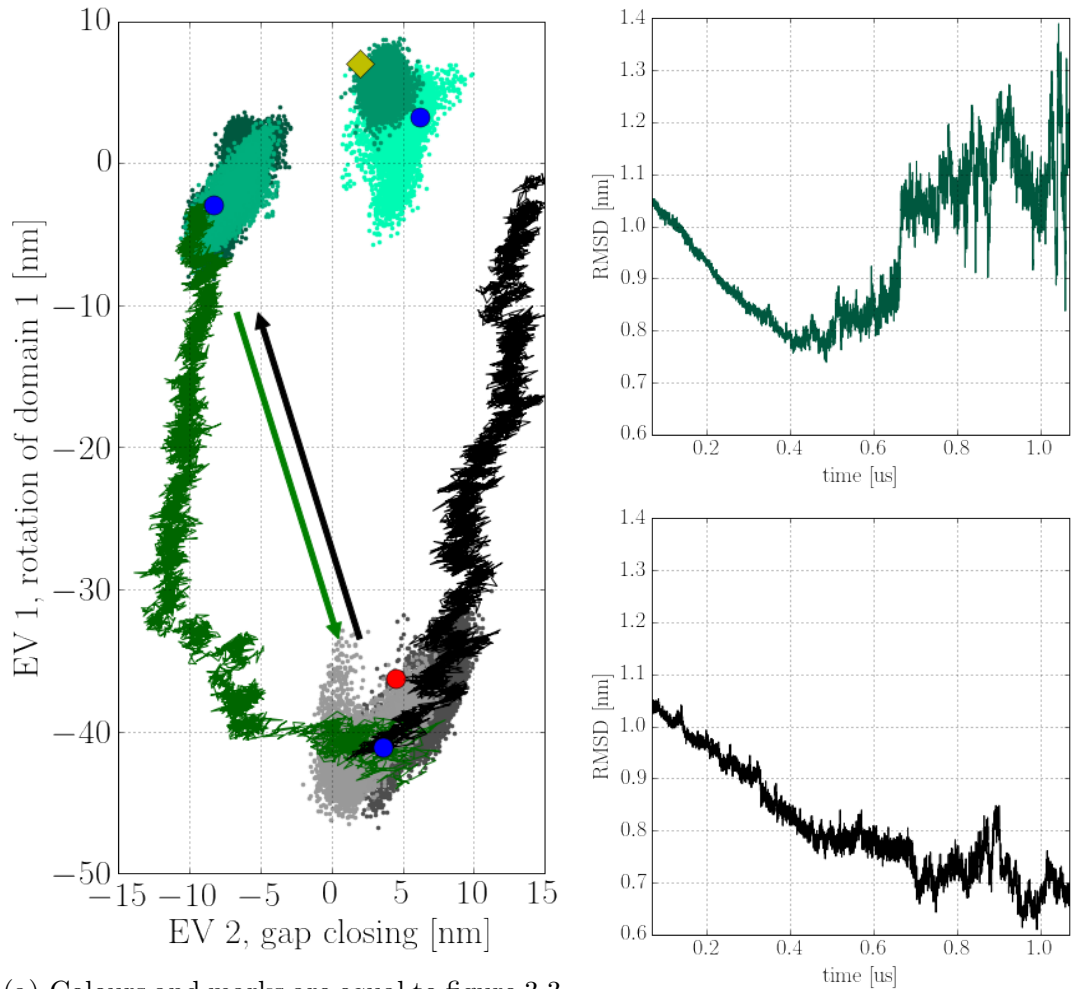
As the simulations of EF-Tu in solution started from the EF-Tu<sub>GDPcrystal</sub> · GDP and EF-Tu<sub>cryo-EM</sub> · GDP as well as the EF-Tu<sub>endpoint</sub> · GDP complexes show no overlap in the plane of the first two eigenvectors (see figure 3.3), the question arises whether these structures are separated by free energy barriers. Such barriers would indicate that the ribosome and tRNA are facilitating these conformational changes. To obtain the free energy landscape between these structures umbrella sampling[41] has been attempted. Umbrella sampling requires a trajectory moving from one

### 3 Results

For almost all pulling simulations the end conformations of the simulations differ vastly from the target structure. Some simulations do not even reach the target structure in the plane of the first two eigenvectors (black line in figure 3.10a), others end with an abruptly increasing RMSD (green line in figure 3.10b). This is likely caused by free energy barriers. Because the pulling potential applies increasing forces on EF-Tu, the time it has to find a pathway around the barrier is limited. With forces increasing too quickly, EF-Tu is pulled into these volumes of conformational space with very high free energy, which results in unphysiological conformations. All simulations exhibiting such behaviour were not used for further analysis.

Only one pulling simulation ended up close to its target, pulling from the EF-Tu<sub>endpoint</sub> · GDP towards the EF-Tu<sub>cryo-EM</sub> · GDP structure. To see if the end structure was stable, the simulation was continued without the pulling potential for 100 ns. The RMSD between the simulation to the target structure, fitted to the target structure, (figure 3.9) remained stable around 0.32 nm. WHAM[25] was used on simulations of 41 sampling points, taken from the pulling simulation in 24. ns steps, to sample the free-energy landscape (figure 3.11) along the trajectory. The landscape shows a minimum at the EF-Tu<sub>endpoint</sub> · GDP structure and increases until it reaches a plateau at the target structure, EF-Tu<sub>cryo-EM</sub> · GDP . Three different time windows of the trajectories of the sampling have been used, the full sampling, the last 50 and the last 100 ns. Using the full window leads to the highest free energy for the end structure, the last 100 ns to the lowest barrier. The first few nanoseconds are likely not equilibrated, causing the resulting free energy to be too high. With only 50 ns on the other hand sampling is likely insufficient. Further, the derived energies are far too high. The energy difference between the structures is of the order of  $100 k_B T$ , with such a slope the free cryo-EM simulations, which started on top of the plateau, should have moved along this pathway rapidly.

Cryo-EM and crystal conformation are too different, pulling along the difference vector is not restrictive enough to lead one conformation to the other. The obtained free energy profiles are unreliable



(a) Colours and marks are equal to figure 3.3.

Blue are the structures used as targets for pulling. (b) RMSD of the two trajectories to their target structures over time.

Figure 3.10: Projection onto the first two eigenvectors and RMSD for two of the six pulling simulations. In black is the trajectory started from the  $\text{EF-Tu}_{\text{GDPcrystal}} \cdot \text{GDP}$  structure targeted at the  $\text{EF-Tu}_{\text{endpoint}} \cdot \text{GDP}$  pulling target, in dark green the opposite way.

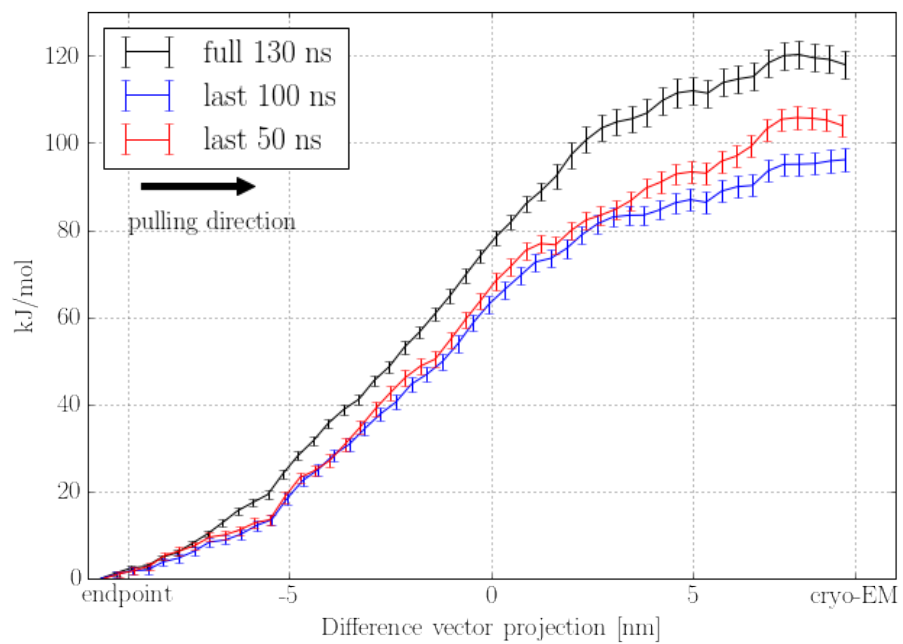


Figure 3.11: Free energy landscape obtained from the WHAM algorithm. The start of the pulling is on the left side, the end structure on the right. Different time windows of the sampling have been used to generate landscapes.

## 4 Conclusion

In this thesis, the molecular mechanism of the antibiotic kirromycin was addressed by studying its effect on the dynamics of EF-Tu using Molecular Dynamics (MD) simulations. EF-Tu delivers aa-tRNA to the ribosome during the elongation step of translation. Kirromycin is known to prevent dissociation of EF-Tu from the ribosome[31]. It is thought to achieve this by obstructing a large scale conformational change of EF-Tu which occurs after GTP hydrolysis in the absence of kirromycin.[37].

To test this hypothesis, MD simulations, provided by Lars V. Bock, started from a cryo-EM structure[13]of the EF-Tu·aa-tRNA·GDP·kirromycin complex bound to the 70S ribosome were analysed. For one of the simulations kirromycin has been removed from the complex. In the simulation with kirromycin, EF-Tu stayed close to the cryo-EM conformation. A crystal structure of the EF-Tu · aa-tRNA · GNP · kirromycin complex [PDB code 1ob2, unpublished] is directly in the explored phase space of the simulation, indicating that the conformation of EF-Tu in the simulation with kirromycin is indeed a GTP conformation.

Without kirromycin, EF-Tu's two major motions that are observed in the simulation are rotations of domain 1 towards domain 3 in two different planes. Kirromycin binds in the gap between these two domains. The one occurring first closes the gap between the domains while also changing the conformation of the kirromycin binding site. Since kirromycin is a rigid molecule, the gap closing rotation is likely sterically prevented with kirromycin bound.

Another difference between GTP and GDP state is the secondary structure of residues 40-62, the switch 1 loop. This loop is a part of the tRNA binding site of EF-Tu and interacts directly with the 5' end of bound amino acyl tRNA[33]. GTP crystal structures exhibit a secondary structure where the switch 1 loop forms two  $\alpha$ -helices. GDP bound structures of EF-Tu show the switch loop in a  $\beta$ -sheet conformation, which is thought to be involved in the dissociation of EF-Tu from the ribosome[2]. It has been further suggested that this loop becomes disordered as

## 4 Conclusion

part of GTPase activation[37]. This disordering would then be expected to occur during simulations with kirromycin as it is a post GTPase activation state. During the simulations with kirromycin the secondary structure of the loop remains stable with two  $\alpha$ -helices. Disordering has been suggested because of low resolutions in experimental structures for the switch 1 loop. In the ribosomal simulations with kirromycin the switch 1 loop is very flexible compared to the rest of EF-Tu's domain 1, this might explain the low resolutions.

If kirromycin holds EF-Tu in a GTP-like conformation, simulations of the cryo-EM structure without kirromycin are expected to cause EF-Tu to change into its GDP conformation. To test this the kirromycin-free simulation was compared to a crystal structure of a EF-Tu  $\cdot$  GDP complex. The end state of the simulation is far away from the GDP state, the largest difference is a rotation of domain 1 against domain 3, similar to the reported difference between GTP and GDP EF-Tu conformations. As the GDP crystal structure is a complex without tRNA and ribosome, the conformational change could occur more rapidly during simulations of the EF-Tu  $\cdot$  GDP complex, taken out of the kirromycin containing cryo-EM structure, in solution. This was tested, but the simulations did not reach the GDP crystal structure. However, simulations of the same conformation with kirromycin bound explored less phase space, further indicating that kirromycin inhibits EF-Tu's dynamics. Further the EF-Tu  $\cdot$  GDP complex was taken from last step of the kirromycin free ribosome simulations and simulated. These simulations did not get close to the GDP crystal structure either. Simulations started from the GDP structure did not reach the GTP cryo-EM conformation. In the EF-Tu  $\cdot$  GDP complex, taken from the cryo-EM structure of the ribosome with GDP and kirromycin, simulations the gap closing motion is no longer observed and the switch 1 loops secondary structure remains stable with two  $\alpha$ -helices. This suggests that the free energy landscape of EF-Tu is altered in the ribosomal complex to allow the conformational change.

To test whether there are free energy barriers preventing the conformational change from structures close to the GTP cryo-EM structure to a structure close to the GDP crystal, umbrella sampling has been used. Between three different states of EF-Tu in solution, the GTP cryo-EM, GDP crystal and the endstate of the kirromycin-free ribosomal complex simulation, simulations have been pulled along the difference vector using a harmonic potential for each pairing in both directions. However, these simulations either ended in unphysiological conformations or did not get close to the target structure. This indicates the existence of free energy barriers on the

path. However, whether these barriers prevent the conformational change is unclear as the pulling might have been simply too fast, preventing EF-Tu from finding a low energy pathway around the barriers. Better approaches would have been to move the potential along other variables, like the cross-correlation or the RMSD. Using the RMSD might however not be a good option for this specific motion either, as the RMSD between simulation and target structure decreasing does not guarantee to get close in the plane of the first two eigenvectors (see figure 3.10, black line).

All in all, different dynamics of the switch 1 loop and differences in dynamics of EF-Tu in solution, and in complex with the ribosome and tRNA, strongly suggest an involvement of the ribosome and the tRNA in the conformational change from GTP to GDP state. Also, the simulations of the ternary complex on the ribosome indicate that kirromycin prevents this conformational change by sterically blocking a rotation of EF-Tu's GTP binding domain 1 towards domain 3.



# Bibliography

- [1] Farhad Abdulkarim, Lars Liljas, and Diarmaid Hughes. Mutations to kirromycin resistance occur in the interface of domains i and iii of ef-tu · gtp. *FEBS letters*, 352(2):118–122, 1994.
- [2] K Abel, MD Yoder, R Hilgenfeld, and F Journak. An alpha to beta conformational switch in ef-tu structure 1996 4. *N*, 10:1153–1159.
- [3] Mark James Abraham, Teemu Murtola, Roland Schulz, Szilárd Páll, Jeremy C Smith, Berk Hess, and Erik Lindahl. Gromacs: High performance molecular simulations through multi-level parallelism from laptops to supercomputers. *SoftwareX*, 1:19–25, 2015.
- [4] MJ Abraham, D Van Der Spoel, E Lindahl, and B Hess. The gromacs development team gromacs user manual version 5.0. 4, 2014.
- [5] Stephen F Altschul, Thomas L Madden, Alejandro A Schäffer, Jinghui Zhang, Zheng Zhang, Webb Miller, and David J Lipman. Gapped blast and psi-blast: a new generation of protein database search programs. *Nucleic acids research*, 25(17):3389–3402, 1997.
- [6] Stephen F Altschul, John C Wootton, E Michael Gertz, Richa Agarwala, Aleksandr Morgulis, Alejandro A Schäffer, and Yi-Kuo Yu. Protein database searches using compositionally adjusted substitution matrices. *The FEBS journal*, 272(20):5101–5109, 2005.
- [7] Herman JC Berendsen, James PM Postma, Wilfred F van Gunsteren, and Jan Hermans. Interaction models for water in relation to protein hydration. In *Intermolecular forces*, pages 331–342. Springer, 1981.
- [8] Herman JC Berendsen, JPM van Postma, Wilfred F van Gunsteren, ARHJ DiNola, and JR Haak. Molecular dynamics with coupling to an external bath. *The Journal of chemical physics*, 81(8):3684–3690, 1984.

## Bibliography

- [9] HJC Berendsen, JR Grigera, and TP Straatsma. The missing term in effective pair potentials. *Journal of Physical Chemistry*, 91(24):6269–6271, 1987.
- [10] Scott C Blanchard, Ruben L Gonzalez, Harold D Kim, Steven Chu, and Joseph D Puglisi. trna selection and kinetic proofreading in translation. *Nature structural & molecular biology*, 11(10):1008–1014, 2004.
- [11] Max Born and Robert Oppenheimer. Zur quantentheorie der molekeln. *Annalen der Physik*, 389(20):457–484, 1927.
- [12] S Cusack, A Yaremchuk, and M Tukalo. The crystal structures of t. thermophilus lysyl-trna synthetase complexed with e. coli trna (lys) and a t. thermophilus trna (lys) transcript: anticodon recognition and conformational changes upon binding of a lysyl-adenylate analogue. *The EMBO journal*, 15(22):6321, 1996.
- [13] Niels Fischer, Piotr Neumann, Andrey L Konevega, Lars V Bock, Ralf Ficner, Marina V Rodnina, and Holger Stark. Structure of the e. coli ribosome–ef-tu complex at  $< 3$  Å resolution by cs-corrected cryo-em. *Nature*, 520(7548):567–570, 2015.
- [14] Joachim Frank. Time-resolved cryo-electron microscopy: Recent progress. *Journal of Structural Biology*, 2017.
- [15] Jason Gans and David Shalloway. Shadow mass and the relationship between velocity and momentum in symplectic numerical integration. *Physical Review E*, 61(4):4587, 2000.
- [16] KB Gromadski and MV Rodnina. Kinetic determinants of high-fidelity trna discrimination on the ribosome. *Molecular Cell*, 13:191–200, 2004.
- [17] Olgun Guvench and Alexander D MacKerell. Comparison of protein force fields for molecular dynamics simulations. *Molecular modeling of proteins*, pages 63–88, 2008.
- [18] Robert W Holley, jean Apgar, George A Everett, James T Madison, Mark Marquisee, Susan H Merrill, John Robert Penswick, and Ada Zamir. Structure of a ribonucleic acid. *Science*, pages 1462–1465, 1965.

- [19] Viktor Hornak, Robert Abel, Asim Okur, Bentley Strockbine, Adrian Roitberg, and Carlos Simmerling. Comparison of multiple amber force fields and development of improved protein backbone parameters. *Proteins: Structure, Function, and Bioinformatics*, 65(3):712–725, 2006.
- [20] Wolfgang Kabsch and Christian Sander. Dictionary of protein secondary structure: pattern recognition of hydrogen-bonded and geometrical features. *Biopolymers*, 22(12):2577–2637, 1983.
- [21] Martin Karplus and J Andrew McCammon. Molecular dynamics simulations of biomolecules. *Nature Structural & Molecular Biology*, 9(9):646–652, 2002.
- [22] Johannes Kästner. Umbrella sampling. *Wiley Interdisciplinary Reviews: Computational Molecular Science*, 1(6):932–942, 2011.
- [23] Ute Kothe and Marina V Rodnina. Delayed release of inorganic phosphate from elongation factor tu following gtp hydrolysis on the ribosome. *Biochemistry*, 45(42):12767–12774, 2006.
- [24] Ute Kothe, Hans-Joachim Wieden, Dagmar Mohr, and Marina V Rodnina. Interaction of helix d of elongation factor tu with helices 4 and 5 of protein 17/12 on the ribosome. *Journal of molecular biology*, 336(5):1011–1021, 2004.
- [25] Shankar Kumar, John M Rosenberg, Djamal Bouzida, Robert H Swendsen, and Peter A Kollman. The weighted histogram analysis method for free-energy calculations on biomolecules. i. the method. *Journal of computational chemistry*, 13(8):1011–1021, 1992.
- [26] Frederick J LaRiviere, Alexey D Wolfson, and Olke C Uhlenbeck. Uniform binding of aminoacyl-trnas to elongation factor tu by thermodynamic compensation. *Science*, 294(5540):165–168, 2001.
- [27] Hubert Maehr, Michael Leach, Thomas H Williams, and John F Blount. The chemistry of aurodox and related antibiotics. *Canadian Journal of Chemistry*, 58(5):501–526, 1980.
- [28] JR Mesters, LA Zeef, R Hilgenfeld, J Martien de Graaf, B Kraal, and L Bosch. The structural and functional basis for the kirromycin resistance of mutant ef-tu species in escherichia coli. *The EMBO journal*, 13(20):4877, 1994.

## Bibliography

- [29] Danesh Moazed and Harry F Noller. Intermediate states in the movement of transfer rna in the ribosome. *Nature*, 342(6246):142–148, 1989.
- [30] Jeffrey K Noel and Paul C Whitford. How ef-tu can contribute to efficient proofreading of aa-trna by the ribosome. *Nature communications*, 7:13314, 2016.
- [31] Andrea Parmeggiani and Guido WM Swart. Mechanism of action of kirromycin-like antibiotics. *Annual Reviews in Microbiology*, 39(1):557–577, 1985.
- [32] Jay W Ponder and David A Case. Force fields for protein simulations. *Advances in protein chemistry*, 66:27–85, 2003.
- [33] PNMKSTGP Reshetnikova, Brian FC Clark, and Jens Nyborg. Crystal structure of the ternary complex of phe-trnaphe, ef-tu, and a gtp analog.
- [34] Marina V Rodnina, Rainer Fricke, and Wolfgang Wintermeyer. Transient conformational states of aminoacyl-trna during ribosome binding catalyzed by elongation factor tu. *Biochemistry*, 33(40):12267–12275, 1994.
- [35] Marina V Rodnina, Kirill B Gromadski, Ute Kothe, and Hans-Joachim Wieden. Recognition and selection of trna in translation. *FEBS letters*, 579(4):938–942, 2005.
- [36] T Martin Schmeing and V Ramakrishnan. What recent ribosome structures have revealed about the mechanism of translation. *Nature*, 461(7268):1234–1242, 2009.
- [37] T Martin Schmeing, Rebecca M Voorhees, Ann C Kelly, Yong-Gui Gao, Frank V Murphy, John R Weir, and V Ramakrishnan. The crystal structure of the ribosome bound to ef-tu and aminoacyl-trna. *Science*, 326(5953):688–694, 2009.
- [38] Friedrich Schotte, Manho Lim, Timothy A Jackson, Aleksandr V Smirnov, Jayashree Soman, John S Olson, George N Phillips, Michael Wulff, and Philip A Anfinrud. Watching a protein as it functions with 150-ps time-resolved x-ray crystallography. *Science*, 300(5627):1944–1947, 2003.
- [39] Annette Sievers, Malte Beringer, Marina V Rodnina, and Richard Wolfenden. The ribosome as an entropy trap. *Proceedings of the National Academy of Sciences of the United States of America*, 101(21):7897–7901, 2004.

- [40] Holger Stark, Marina V Rodnina, Hans-Joachim Wieden, Friedrich Zemlin, Wolfgang Wintermeyer, and Marin van Heel. Ribosome interactions of aminoacyl-trna and elongation factor tu in the codon-recognition complex. *Nature Structural & Molecular Biology*, 9(11):849–854, 2002.
- [41] Glenn M Torrie and John P Valleau. Nonphysical sampling distributions in monte carlo free-energy estimation: Umbrella sampling. *Journal of Computational Physics*, 23(2):187–199, 1977.
- [42] DH Tsai. The virial theorem and stress calculation in molecular dynamics. *The Journal of Chemical Physics*, 70(3):1375–1382, 1979.
- [43] Loup Verlet. Computer" experiments" on classical fluids. i. thermodynamical properties of lennard-jones molecules. *Physical review*, 159(1):98, 1967.
- [44] Lutz Vogeley, Gottfried J Palm, Jeroen R Mesters, and Rolf Hilgenfeld. Conformational change of elongation factor tu (ef-tu) induced by antibiotic binding crystal structure of the complex between ef-tu · gdp and aurodox. *Journal of Biological Chemistry*, 276(20):17149–17155, 2001.
- [45] Göran Wallin, Shina CL Kamerlin, and Johan Åqvist. Energetics of activation of gtp hydrolysis on the ribosome. *Nature communications*, 4:1733, 2013.
- [46] Albert Weijland, Kim Harmark, Robbert H Cool, Pieter H Anborgh, and Andrea Parmeggiani. Elongation factor tu: a molecular switch in protein biosynthesis. *Molecular microbiology*, 6(6):683–688, 1992.
- [47] Daniel N Wilson. Ribosome-targeting antibiotics and mechanisms of bacterial resistance. *Nature reviews. Microbiology*, 12(1):35, 2014.
- [48] H Wolf and H Zähler. Stoffwechselprodukte von mikroorganismen. *Archives of Microbiology*, 83(2):147–154, 1972.
- [49] Heinz Wolf, Gianni Chinali, and Andrea Parmeggiani. Kirromycin, an inhibitor of protein biosynthesis that acts on elongation factor tu. *Proceedings of the National Academy of Sciences*, 71(12):4910–4914, 1974.



# Acknowledgements

I would like to thank my supervisor Prof. Helmut Grubmüller for the opportunity to work on a very interesting project and providing guidance where needed. Further I would like to thank Lars V. Bock for the patience to answer my every question and many fruitful discussions about the project.

Last but not least I want to thank all the other members of the department for theoretical and computational biophysics for their help, be it through asking questions during seminar presentations, solving of technical issues, administrative work or any other way.

**Erklärung** nach §18(8) der Prüfungsordnung für den Bachelor-Studiengang Physik und den Master-Studiengang Physik an der Universität Göttingen:

Hiermit erkläre ich, dass ich diese Abschlussarbeit selbständig verfasst habe, keine anderen als die angegebenen Quellen und Hilfsmittel benutzt habe und alle Stellen, die wörtlich oder sinngemäß aus veröffentlichten Schriften entnommen wurden, als solche kenntlich gemacht habe.

Darüberhinaus erkläre ich, dass diese Abschlussarbeit nicht, auch nicht auszugsweise, im Rahmen einer nichtbestanden Prüfung an dieser oder einer anderen Hochschule eingereicht wurde.

Göttingen, den November 11, 2017

(Malte Varias)